heliotek
DIVISION OF TEXTRON ELECTRONICS, INC.

EMpire 5-6301, Area Code 213
TWX No. 213 464-5978
12500 GLADSTONE AVE., SYLMAR, CALIFORNIA

Manufacturer of Space Age Solid State Devices

Hard copy (HC) $4.00

Microfiche (MF) $1.00

1.0	Report No.	Project No.	Date
	19	NAS5-3558	10 January 1965

2.0 Title: Final Report
Development of an Improved Radiation Resistant Solar Cell.

3.0 Written By: P. Berman and W. Kiba

4.0 Approved By: E. L. Ralph

5.0 Status: Preliminary____ Planning____
Pretest____ Progress____ Final X Revision____

6.0 Summary

A complete process summary for fabrication of drift field cells is presented. Problem areas and attempts to eliminate or circumvent these areas are discussed. The electrical and spectral characteristics of all sample cells submitted during this contract are presented. Comparisons between theoretically expected and experimentally obtained values for the important cell parameters are discussed and analyzed. The results of radiation experiments performed by NASA Goddard are also analyzed.

7.0 Circulation: 1 copy to Contracting Officer, NASA
5 copies to Technical Representative, NASA
1 copy to Electro-Optical Systems, Inc.
1 copy to Texas Instruments, Inc.
9 copies Heliotek

TABLE OF CONTENTS

REFERENCES

(1) Wolf, M., "Drift Fields in Photovoltaic Solar Energy Converter Cells", Proceedings of the IEEE Vol. 51, No. 5, May, 1963.

(2) Berman, P., Transitron Electronic Corp., "Radiation Damage in Silicon Solar Cells Using 750 KeV and 2 MeV Electrons", October 1960.

(3) Mandelkorn, J., Schwartz, L., Broder, J., Kautz, H. and Ulmar, R., "Effects of Impurities on Radiation Damage of Silicon Solar Cells". NASA Technical Memorandum NASA TM X-52007, 1964.

(4) Lang, G. A., T. Stavish, "Chemical Polishing of Silicon with Anhdrous Hydrogen Chloride" RCA Review, December 1963.

(5) M. Wolf and M. B. Prince, "New Developments in Silicon Photovoltaic Device and Their Application in Electronics", J. Brit. IRE, Vol. 18 October, 1958.

(6) R. H. Kingston, "Switching Time in Junction Diodes and Junction Transistors", Proc. of the IRE, Vol. 42, No. 5, May 1954

OBJECTIVE OF CONTRACT

The goal of this contract is to produce a type of solar cell which will be capable of good performance after long exposure to space radiation. The objective is to be achieved by the introduction of a drift field into the cell using the best solar cell technology currently available. The drift field will be incorporated by designing and fabricating a suitable impurity concentration gradient within the cell. Epitaxial growth techniques will be employed to provide the required concentration gradient.

Since the basic design and techniques utilized in the fabrication of the drift field cell were well known prior to the inception of this contract, the contract objective is the refinement of these techniques rather than the investigation and innovation of new technologies.

I. ABSTRACT and SUMMARY

Heliotek has been investigating the problem of radiation damage on solar cells for several years, and in particular it has been working on a new cell design utilizing a drift field in the base region. The first consideration given to this cell design was a theoretical analysis of various drift field cell configurations and of their performance after various radiation dosages to determine what improvements, if any, could be obtained through utilization of a drift field in the base region of a solar cell. It was found, on the basis of an extensive theoretical study by M. Wolf[1], that indeed significant improvement could be obtained through utilization of a drift field with optimized width and field strength for a particular radiation environment. The next consideration was the development of a fabrication method which would make it possible to attain these predetermined optimum parameters. Heliotek conceived a new approach for fabricating drift field cells using an epitaxial technique, and performed preliminary experimentation to prove feasibility. The objective of this contract was to further develop the state-of-the-art of this cell. The first phase (6 months) of this contract has been devoted to the improvement of the methods and techniques used in the fabrication of the drift field solar cell.

The process currently being used may be broken down into 4 major steps.

1. Preparation of a substrate wafer.
2. Epitaxial deposition of back up material and subsequent formation of the drift field region.
3. Lapping and etching for removal of the excess substrate material.
4. Fabrication of the active solar cell (i.e., junction formation, contact application, etc.).

---

(1) Wolf, M., "Drift Fields in Photovoltaic Solar Energy Converter Cells", Proceedings of the IEEE Vol. 51, No. 5, May 1963.

The first step includes the selection of the ingots which will be utilized in the fabrication of the drift field cell. In order to take advantage of past experience concerning the radiation resistance properties of solar cells[2], the basic N^+/P solar cell structure is utilized. Thus, the substrate material is silicon single crystalline P type, with a resistivity of 10 ohm cm or greater. In order to assure that ingots utilized in the fabrication of the drift field cell are capable of yielding solar cells with good electrical characteristics at least 10 non-drift field cells are fabricated from blanks cut from the ingots. These non-drift field (normal production type) cells serve a twofold purpose in that they evaluate the potential electrical performance of the ingot and they subsequently can be utilized in radiation experiments to determine precisely how much additional radiation resistance has been attained by inclusion of the base region drift field. This latter purpose is quite important since it is well known that the radiation resistance of a solar cell is strongly dependent upon the material from which the cell is fabricated[3]. The remaining portion of the ingot is sliced into discs and fabricated into drift field solar cells. After both types of cells are fabricated, a direct comparison of electrical outputs can be made.

The second major steps are the epitaxial deposition and the formation of the drift field region. The epitaxial deposition involves surface preparation of the substrate slices by chemical etching carbon masking of the back surface of the substrate, deposition of heavily boron doped silicon, and evaluation of the epitaxial layer. The drift field region is then formed by diffusion of the boron atoms from the

(2) Berman, P, Transitron Electronic Corp., "Radiation Damage in Silicon Solar Cells Using 750 KeV and 2 MeV Electrons", October 1960.

(3) Mandelkorn, J., Schwartz, L., Broder, J., Kautz, H. and Ulmar, R., "Effects of Impurities on Radiation Damage of Silicon Solar Cells". NASA Technical Memorandum NASA TM X-52007, 1964.

thick epitaxial layer into the substrate material with lower impurity concentration. This diffusion is currently being done in a tube furnace at a temperature of 1200°C for a period of 5 hours. The slices are then mounted on ceramic cutting blocks using a hard wax and are cut to size on a diamond saw.

The third major step consists of reduction of the substrate material to the material to the desired thickness of about 1.0 mils (25μ). The surface being lapped or etched must be parallel to the interface of the substrate and epitaxial layer and must be of accurately controlled thickness in order to locate the N^+/P junction in the proper relation to the base region drift field.

In the fourth step, fabrication of the active cell starts with a phosphorus diffusion to form the N^+/P junction of the cell. This diffusion is performed at about 900°C for 20 minutes and locates the junction at about 0.3 microns below the surface of the substrate. From this point on the drift field cells are processed by standard techniques forming the contacts, etching the edges and applying an antireflection coating.

During the first phase of the contract several materials were used to mask the back side against the etching and undergrowth which occurs during the epitaxial process. An attempt to use a thermoxide layer for a mask was successful for thin deposits, however the oxide layer would not withstand the etching and undergrowth for the required thicker deposits. Consequently alternate methods of masking were investigated. A carbon black layer was found to give the desired masking effect. The carbon layer is deposited by holding the slice surface over the flame of a candle until a smooth coat of carbon black is deposited over the entire face of the slice. Two such carbonized slices are stacked with carbon side against carbon side. The stack is placed into the epitaxial reactor, with the slice on which the deposit is to be made placed on the top.

During the first phase, a modification was made to the epitaxial system and a 5 KW RF generator was added. To utilize the RF generator's advantages over a resistance heater, the reactor assembly was also modified, resulting in a usable heat zone which was about 200% greater than that previously obtained with the resistance heater.

Certain modifications of the process were investigated during the second phase. A method for final reduction of substrate thickness by etching was studied in order to minimize strains at the epitaxial substrate interface. Various types of etchants were investigated and the most advantageous etch was found to be a composition of 2:1:1, HNO_3HF:CH_3COOH. Some difficulties were encountered with cells which were found to be locally shorted, possibly due to the etching of minute pits which extended into the epitaxial regions, but a number of cells were successfully fabricated by using a tilted, rotating container to provide uniform agitation to the cell. Other modifications included the utilization of a gradual heating and cooling cycle during the epitaxial deposition in order to minimize strains which could cause slice bowing, the utilization of a larger silicon tetrachloride reservoir in order to maintain a steady growth rate during the long epitaxial runs necessary to deposit layers which are 10 mils thick or greater, and the utilization of larger area substrate in order to obtain greater material utilization.

An experimental and theoretical analysis of drift field cells which had poor curve shape and low open circuit voltage was made. By means of control cells which are always utilized in the fabrication of drift field cells, poor material and/or N/P junction diffusion were ruled out as a possible cause of the poor cell characteristics. Actual series and shunt resistance measurements showed that these parameters were not responsible for the poor electrical characteristics. A measurement of the A-factor which occurs in the exponential of the diode equation indicated that the A-factor seems to be somewhat lower in value than normally obtained from field-free cells.

This may be due to processing since, on the basis of theory, the reverse saturation current of the drift field cells should actually be lower than that of the field-free cells because of the larger number of ionized impurity atoms present in the former cell type.

Analysis of spectral characteristics of the drift field cells showed that they are quite uniform from cell to cell. Some theoretical consideration of the relationship between cell short circuit current in various light systems, specifically tungsten and m=0 sunlight systems, are presented in this report. A comparison was made between the experienced short circuit currents and those which were predicted for a drift field cell having a design similar to the one being utilized in this contract. Theoretically one would expect a short circuit current decrease of about 20% and this was shown to be in quite good agreement with the currents actually being obtained from the drift field sample cells. A rough theoretical calculation of the value of open circuit voltage which may be expected from drift field cells indicated that V_{oc} may be as much as .075 volts over that obtained in the field free cells, due primarily to the additional ionized impurity atoms introduced by the field diffusion. The open circuit voltages of the actual sample cells have not shown this to be the case in practice. In fact, the open circuit voltages of the drift field cells are usually lower than those of the field-free control cells. The estimated V_{oc} increase did not take into account the spatial variation of the parameters involved and may be too optimistic; however, the fact that some drift field cells do exceed the field-free control cells in open circuit voltage indicates that the other cells are falling below their potentiality with respect to this parameter.

Thus far cells from three sample lots have undergone bombardment by 1 MeV electrons up to flux levels of the order of 10^{16} e /cm^2. The cells which were irradiated were selected from sample lots one, three and four. The data obtained by NASA indicates that the cells selected from the third and fourth lots did not have the same radiation characteristics as did the cells from the first lot which had been irradiated in a previous series of experiments. Cells from the first lot showed the best radiation characteristics and indicated almost

no current degradation over the flux range considered, while those from the fourth lot exhibited the least radiation resistance. A very interesting observation was made that seemed to be generally true for all cells considered in these experiments; namely, the greater the resistance of short circuit to radiation damage, the poorer is the resistance of open circuit voltage to damage by radiation. It is postulated that this is a function of the distance between the edge of the base region drift field and the electrical p-n junction, although the nature of the function is yet unknown.

II. INTRODUCTION

In the theoretical analysis of the drift field type solar cell, the general solar cell theory applies after the introduction of certain modifications which are associated with the drift field. In the case of the drift field cell, collection on both sides of the junction is assisted by acceleration of the generated minority carriers toward the junction by action of the drift field. In the standard type solar cell such a mechanism is effective only in the diffused layer below the exposed surface while collection below the junction, (i.e., in the base region) is based solely on diffusion of the minority carriers towards the junction. Although this mechanism is very efficient in crystals which have a sufficiently long minority carrier lifetime, particle radiation, which decreases minority carrier lifetime, can severely reduce the junction collection efficiency and hence the cell power output. A properly designed solar cell with a drift field in the base region reduces the dependency of good current collection on minority carrier lifetime for a certain range of such lifetimes and thus it is expected that cell power degradation due to radiation damage will be reduced. In order to intelligently approach the design problems, consideration must be made of the factors which affect solar cell radiation resistance as well as those which affect cell efficiency. This involves analysis of the effect of the drift field on the junction collection efficiency as a function of minority carrier lifetime, and of the effect of the field on the other solar cell parameters.

About a year and a half ago, Heliotek originated a novel approach to fabricate a drift field solar cell embodying the optimum design parameters. This approach appears to be a very feasible process with the advantage that the problem areas comprise only the development of uncomplicated chemical and mechanical processing techniques rather than highly sophisticated new approaches. A description of the cell design is shown in Fig. 1. In this design an epitaxial technique is utilized, however the important factor to consider is that this epitaxial region A is an essentially passive region. This means that it does not make

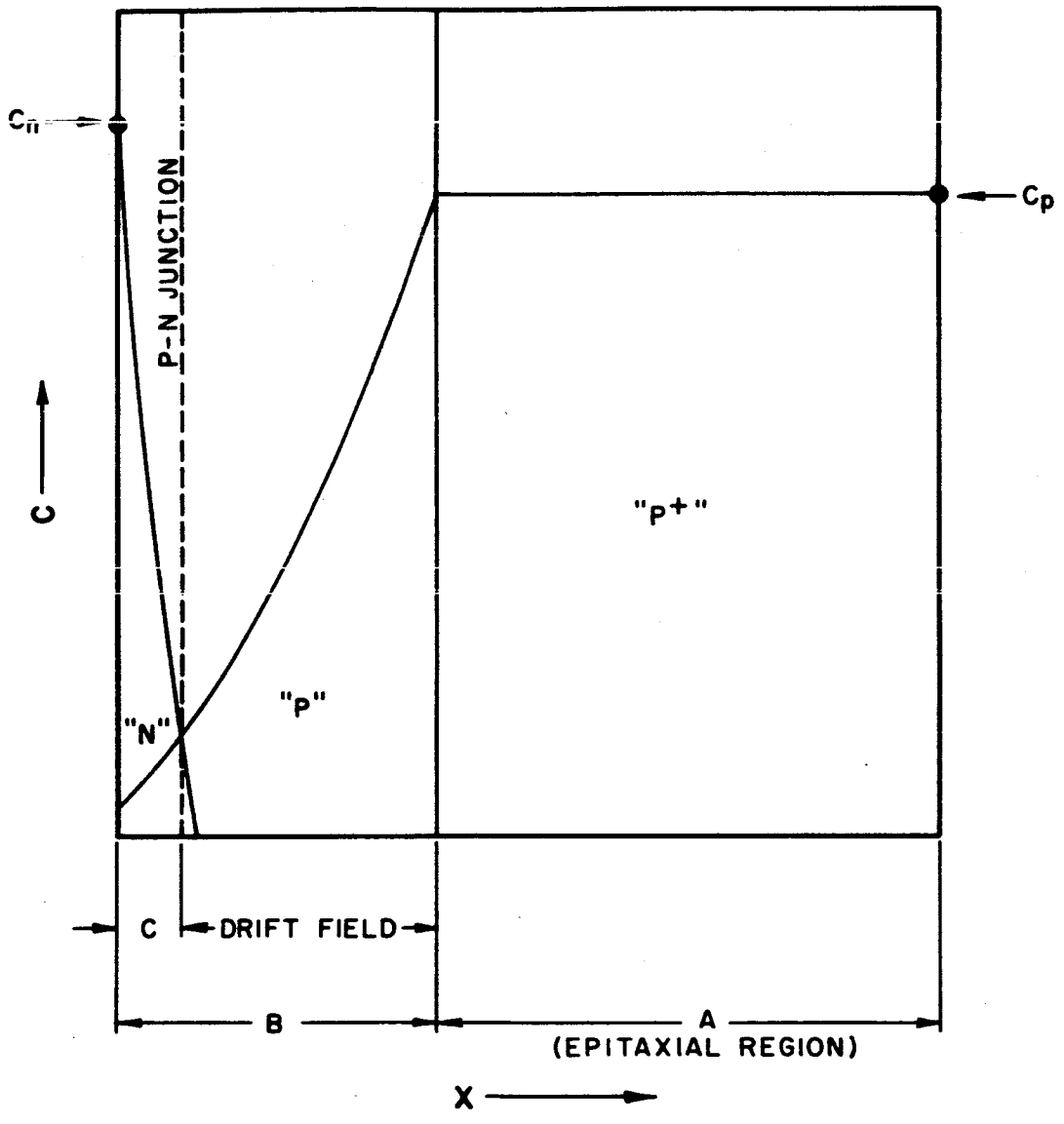

FIG. 1

T-2202

any significant contribution to the current collected or have any active part in the junction electrical characteristics except for the effects of series resistance. The junction and the drift field are both formed in region B which is the substrate crystal which can be of high perfection single crystal silicon known to be capable of yielding high efficiency solar cells. The material being used is high resistivity P type silicon. A relatively thick (~10 mil) slice of this material is used as the starting material for the drift field cell. A heavily doped P type epitaxial layer is then deposited on this substrate. At present the layer is single crystalline in structure, however it is possible that eventually a polycrystalline deposition can be utilized since the major purpose of the epitaxial layer is to add mechanical support to the slice through increased thickness without significantly increasing the series resistance, and to act as a source of dopant for the base region drift field. Obviously either single or polycrystalline material would be sufficient to qualify for both of these characteristics. Single crystalline epitaxial depositions have been utilized thus far to avoid any lattice stresses introduced because of a crystal mismatch which could tend to crack the slice during subsequent operations. The epitaxial layer is built up to a suitable thickness (Region A, Fig. 1) of about 8 to 10 mils so that a relatively strong, rugged cell can be obtained. The drift field is then formed in the single crystal material by diffusing the P type impurities from the epitaxial region into the high resistivity single crystal region. This diffusion is done prior to reducing the single crystal region to thickness B. Then the single crystal substrate is reduced in thickness by lapping and etching techniques. The thickness B (Fig. 1) for optimum collection and performance, should be about 0.5 mils (12μ).

After the single crystal substrate is reduced to thickness B, the P-N junction is formed below the cell surface by standard phosphorus diffusion techniques with a junction located at a depth C (Fig. 1) of about 0.3 microns typical for a blue response type space cell.

In the fabrication of the drift field cell, the diffusion steps are done separately for better control of impurity concentration profiles and for easier analysis of the fabrication procedure. By this technique the impurity gradient of the P type impurity can be varied over at least 4 orders of magnitude, as is required by the theory. Standard ohmic contacting and gridding techniques are applied to complete the electrical contacts of the cell.

As a first design, the single layer model described by Wolf having an electrostatic potential difference of 0.118V across an 0.5 mil (12μ) drift field region is being made.

III. FABRICATION PROCESS

1.0 FABRICATION PROCESS OUTLINE AND SUMMARY

In order to fabricate the drift field cell, the following process steps are currently being used. A P type, single crystalline ingot having a resistivity of 10 ohm cm or greater to be used as substrate material is selected. A portion of the selected ingot is cut and fabricated into standard N^+/P (1 x 2 cm) solar cells to be used as control cells. The remaining portion of the ingot is sliced into discs which are fabricated into drift field solar cells. After both types of cells are fabricated, a direct comparison of electrical outputs can be made since both are prepared from the same ingot.

Fabrication of the drift field cell from the discs is as follows:

Step 1) After cutting, the slices are lapped so that side A is parallel to side B. (Fig. 2). The slices are then cleaned, and polished etched in a heated (90°C) basic etch solution. The basic etch solution consists of 10 gram NaOH, 15 grams $NaNO_3$ and 100 mL of water. For a more detailed description on lapping refer to the Lapping Technique Section, Section 2.

Step 2) In order to mask against the undergrowth of epitaxial silicon on the back side of the substrate (Side B) a carbon mask is used (Fig. 3). The carbon is deposited by holding the slice with the face to be masked over the flame of a paraffin candle until a smooth coat of carbon black appears over the entire face of the slice. For each substrate upon which a deposition is to be made, a carbonized back up slice is used. The 2 slices are stacked carbon side to carbon side and placed on the reactor heater. The combination of the carbon mask plus the back up slice gives a very effective mask with essentially no undergrowth or etching.

Step 3) A "P" type epitaxial layer having an impurity concentration of about 10^{20} boron atoms/cm^3 and a thickness of approximately 10 mils, is deposited on side A (Fig. 4). The epitaxial layer serves as back up material and dopant source for the very thin drift field cell. To

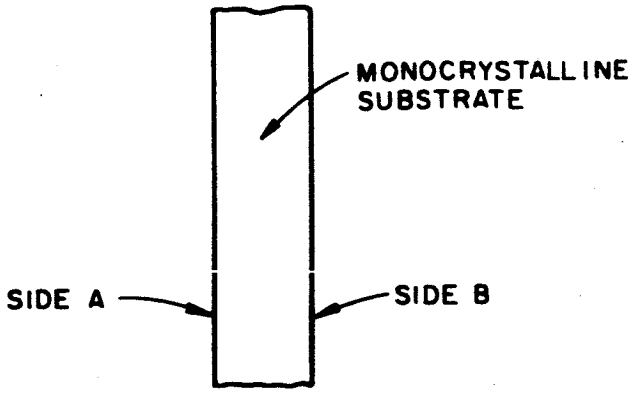

FIG. 2

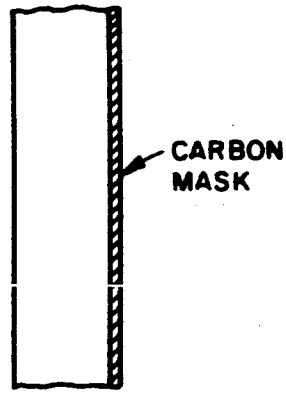

FIG. 3

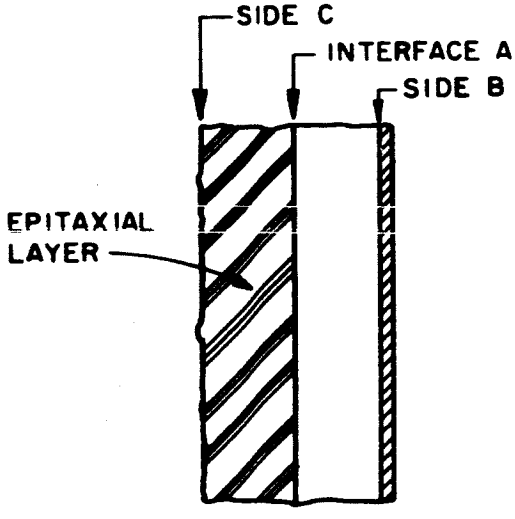

FIG. 4

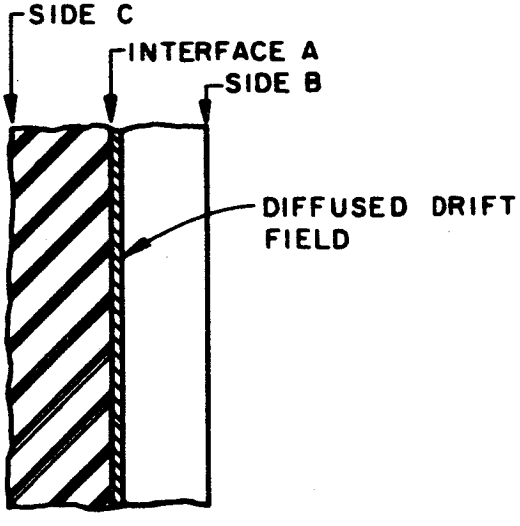

FIG. 5

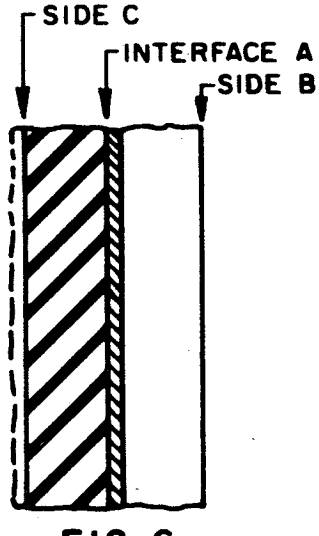

FIG. 6

T-2379

determine the thickness of the deposited layer, a metallographic cross section of a chip taken from the slice after deposition is made and evaluated. (Refer to the Evaluation Technique Section for more details regarding cross sections and staining techniques.)

Step 4) Diffusion of the boron atoms into the monocrystalline substrate to form the drift field (Fig. 5) is performed at 1250°C for 1 hour 45 minutes. The field depth at this diffusion time and temperature is approximately 10μ (0.4 mils). The highly doped (10^{20} atoms/cm^3) epitaxial layer is used for the dopant source. The diffusion occurs across the interface A into the substrate material which has a uniform boron impurity concentration of about 10^{15} atoms/cm^3, resulting in an impurity gradient referred to as the drift field. To check the drift field width, a cross section of a chip taken from the slice after diffusion is made, delineated, and measured. (Refer to Section Evaluation Technique for more information on cross section and staining techniques.)

Step 5) After diffusion of the drift field region, the slice is then remounted on a lapping fixture and lapped. This lapping is performed on Side C (Fig. 6) to bring the surface plane parallel to side B. Side B is again used as a reference plane as in Step 1.

Step 6) The slice is then mounted, using a hard wax, on a ceramic cutting block, and is sliced to obtain the cell blank dimensions.

Step 7) After the slices have been cut into cell blanks, Side B is then lapped, or lapped and etched down (Fig. 7) using Side C as reference, to obtain a substrate thickness of about 1.0 mils or 25μ. The method of removal of Side B depends on which type of electrical contacts are to be used. The electroless nickel plated contacts require a lapped surface for best adhesion. The sintered titanium silver contacts require a polished etched surface. Again, a cross section is made to verify that the proper thickness of the substrate was obtained. This step is the most critical and the most difficult in the fabrication of the cell.

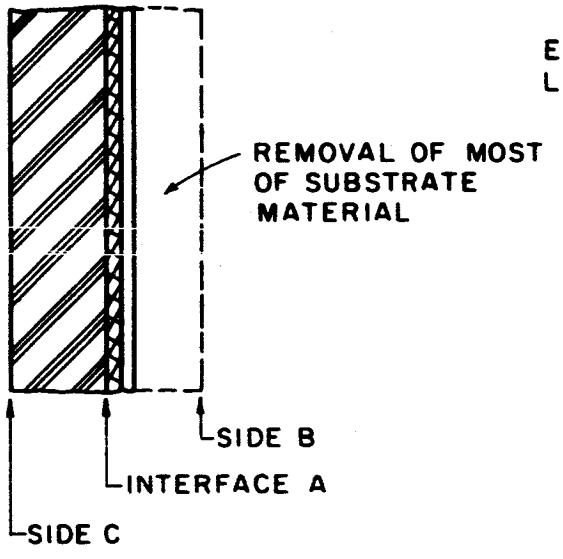
REMOVAL OF MOST
OF SUBSTRATE
MATERIAL
SIDE B
INTERFACE A
SIDE C

FIG. 7

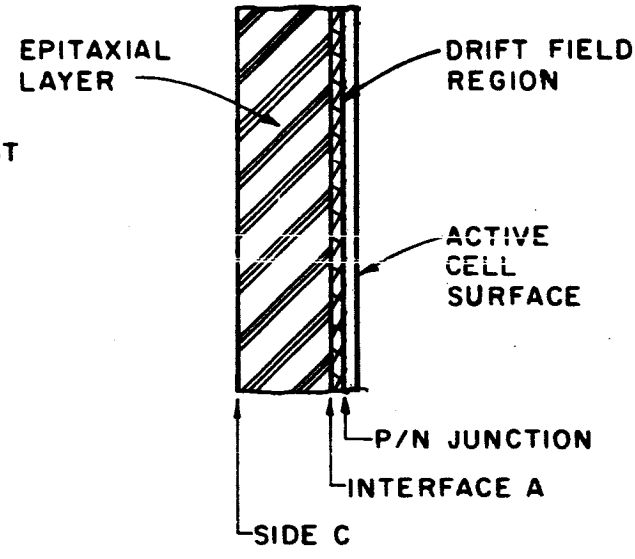
EPITAXIAL
LAYER
DRIFT FIELD
REGION
ACTIVE
CELL
SURFACE
P/N JUNCTION
INTERFACE A
SIDE C

FIG. 8

Step 8) The slice is removed from the lapping fixture, cleaned and diffused using a phosphorous dopant source to form the N^+/P junction at the active cell surface (Fig. 8). This diffusion is performed at about 900°C for 20 minutes, thus forming the junction at about 0.3 microns below the cell surface. This depth will correspond to the best blue response cells presently available.

From this point, the cells are processed by standard techniques to obtain electrical contacts and an antireflection coating is applied.

2.0 LAPPING TECHNIQUE

All of the plane parallel lappings are currently being done on a specially designed lapping fixture. This fixture has three adjustable diamond points protruding from a flat steel disk. The reference side of the slice is mounted flat on the steel disk with a thin layer of a beeswax and resin mixture. This operation is very critical because the uniformity of the wax layer will determine the plane parallelism of the surfaces (A and B, Fig. 2; B and C in Fig. 6). The adjustable diamond points are then set to a predetermined height. The predetermined height is the sum of the desired thickness of the slice plus the thickness of the wax used to secure the slice on the fixture. The thickness of the wax layer is found by measuring the thickness of the slice before and after mounting on the lapping fixture. The thickness measurements and the diamond point height measurements are made by using a Starrett dial indicator and a toolmaker's flat. After all the adjustments and measurements are performed, the actual lapping is done by hand, using graduated grit sizes of silicon carbide lapping compound on a glass plate. When the slice is lapped to the predetermined thickness the diamond points are in contact with the glass lapping plate, thus preventing further grinding of the slice. The last portion of the lapping is done using a 1600 grit lapping compound.

3.0 MASKING AGAINST ETCHING AND UNDERGROWTH

In order to fabricate the drift field cell by the technique proposed by Heliotek, the back surface of the substrate slice must be protected against the etching and crystal deposits which occur during the epitaxial deposition in Step No. 3 of the Fabrication Process section.

Figure 9 is a cross section of a slice not properly protected, showing the deposited layer at the edge of the substrate. It can be seen that the growth is not restricted to the top surface, but also deposits to some extent on the back side (bottom of photo). This undergrowth must be eliminated, since the back surface of the substrate is used as a reference plane during the removal of a portion of the substrate material (Steps 5 and 6 of the Fabrication Method section). The finished active surface of the solar cell should be as plane parallel as possible to the interface between the substrate and the epitaxial material in order to obtain a solar cell with uniform characteristics over its entire area.

Several materials were tested for use as a mask against the undergrowth. The first attempt involved a coating of silicon monoxide deposited on the back side of the substrate. This technique was considered because of the speed with which such oxides can be deposited, however it was not successful due to the fact that the crystal growth was able to penetrate through and nucleate on the SiO mask and to form a very tenacious layer of silicon over the oxide.

Several experiments were also made using a thermal oxide layer as a mask. The first experiment consisted of 3 runs. All slices investigated were polished on one side and lapped on the other. The thermal oxide was grown at 1100°C for 3 hours with an oxygen flow of approximately 1 L/Min. After the oxide layer was grown, half of both faces of the slices were masked with Mylar tape. The slice was then etched in hydrofluoric acid

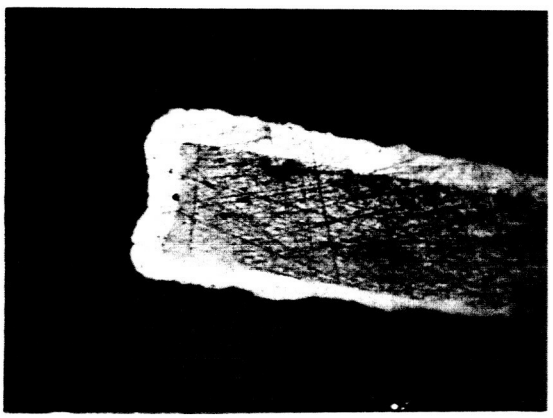

Fig. 9

X 50

to remove the oxide mask from the exposed portions of the slice so that the effectiveness of the mask could be easily analyzed. In each of the 3 runs, 2 slices were used. One slice was placed on the heater with the polished side up and the other with the polished side down, so that both lapped and polished conditions could be studied.

The thermal oxide mask on the back (or bottom) side of the substrates resisted the etch and undergrowth for all 3 experimental runs. The surfaces in Fig. 10 are the microphotographs of the polished sides. The surface in photo A was placed face down (facing heater surface). The left half of photo A is the side which was oxide masked. It can be seen that after silicon deposition and subsequent removal of the oxide the surface remained polished, showing that the oxide provided the desired protection. The right side, which was unprotected by a thermal oxide mask, was exposed and shows signs of etching. Photo B shows the surface of the slice which had the polished face up away from the heater during the deposition process. The masked half of the slice is the dark area on the left and the exposed half is shown on the right. Silicon deposited over the oxide mask, was polycrystalline, and could not be removed in hydrofluoric acid.

The lapped surfaces of both slices did not give useful information because the surfaces were rough enough to nucleate a polycrystalline growth over the oxide which could not be removed. The deposited silicon layers used in the oxide experiments were 0.5 mils to 1 mil thick.

In the second thermal oxide experiment, 2 methods of using the oxide mask were investigated. One method was to place the slice directly on the heater sheath surface with the masked side down. The other method was to place the oxide surfaces of 2 slices face to face. The bottom slice was positioned on the heater surface oxide side up, and the slice upon which the epitaxial layer was to be deposited was placed directly over the bottom slice, oxide side down. Four runs were made

Photo A

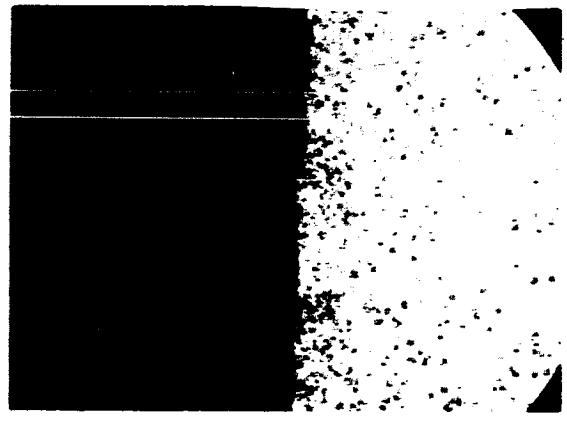

Photo B

utilizing the 2 masking methods on both lapped and polished samples. In all cases where a heavy silicon deposit was obtained there were areas of undergrowth which could not be removed without damaging the slice itself.

It was found that the above masking technique using a thermal oxide layer was not successful in protecting the surface when deposited silicon layers greater than 3 mils were attempted. The surface shown in Fig. 11 is of an oxide layer after a thick deposition of silicon was deposited on the opposite side. The spots on the left side are silicon crystals that have nucleated from the surface of the slice, either through the oxide mask or through holes that were etched through the oxide mask during the deposition period. These growths could not be removed in HF to leave the original polished flat surface as desired.

A third technique utilizing a different material as a mask was tried next. In this case an attempt was made to use carbon as the mask. This approach was successful and provided the desired masking effect. The carbon was deposited by holding the slice with the face to be masked over the flame of a paraffin candle until a smooth coat of carbon black deposit appeared over the entire face of the slice. Six epitaxial runs were made using this carbon mask technique. In each run, 3 carbonized slices were used. One was placed directly on the heater surface, carbon side down while the remaining 2 slices were stacked carbon side against carbon side and placed on the heater. Epitaxial growth of 8 to 12 mils thickness were deposited on these slices.

To better show the masking effect, 2 carbonized slices were placed onto another slice leaving an exposed rectangular area of about 30 mils in width. A 5 mil thick epitaxial growth was deposited onto this rectangle. The growth is the vertical dark strip in the center of Photo No. 12. The fact that no growth was found outside of the rectangular (exposed) area shows the excellent masking qualities of the carbonized silicon slice method.

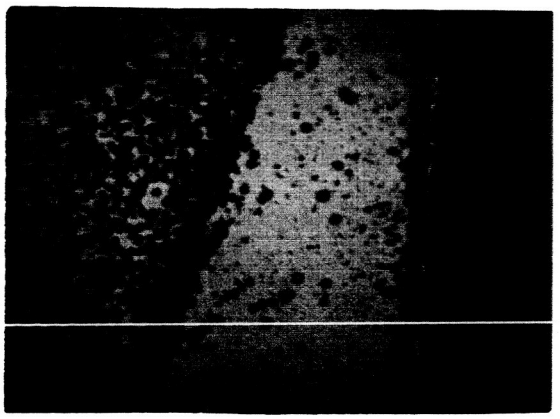

Fig. 11

x 50

Fig. 12

x 50

In order to separate the top slice from the bottom slice in the stack method, it is necessary to grind away the deposited silicon on the periphery of both slices and allow them to remain in an ultrasonically agitated alcohol bath until they separate. This step also removes the carbon mask from the surface of the slice.

4.0 EPITAXIAL TECHNIQUES

The epitaxial system that is being used for this contract was designed and built by Heliotek. The system is constructed of Pyrex, quartz and Teflon in such a manner that contamination is reduced to a minimum. The reactor assembly consists of a quartz tube which is sealed by "O" rings to an end cap. The end cap has an exhaust port where hydrogen carrier gas is burned off. All gas flows are regulated by means of stainless steel valves and are measured with flowmeters. Resistance heating was used in the epitaxial reactor for the first 3-1/2 months of the contract. The heater assembly (Fig. 13) consisted of a quartz sheath which housed a graphite heater. This sheath isolated the heating element completely from the pyrolytic reaction, thus preventing possibilities of contamination from the graphite heater. The cells on which the deposit was to be made were placed on top of the sheath directly above the heating element. During the fourth month of Phase I a 5 KW, 450 KC RF generator was purchased and installed to replace the resistance heater and power supply previously used in the epitaxial system. The reason for the conversion was to obtain a larger and more uniform heat zone. Placement of the new heater system can be seen in Fig. 14. The RF generator is shown on the left, and the induction coil around the reactor chamber tube is shown to the right. The first 8 epitaxial runs which utilized RF heating were made by induction coupling to a 6 x 1-3/4 x 3/8 inch graphite block, which was inserted into the quartz heater sheath formerly used with the resistance heater (see Fig. 13 for heater sheath). It was determined that there were several problems incurred by using the quartz sheath. The major problem encountered was that after several thick epitaxial deposition runs (of approximately 10 mils thickness), much of the quartz would crack away from both the bottom and top surfaces of the quartz sheath upon cooling. This effect was due to the adhesion of deposited silicon to the quartz which resulted in strains introduced during cooling from the elevated temperatures because of differences in thermal expansion coefficients. This problem was not encountered when

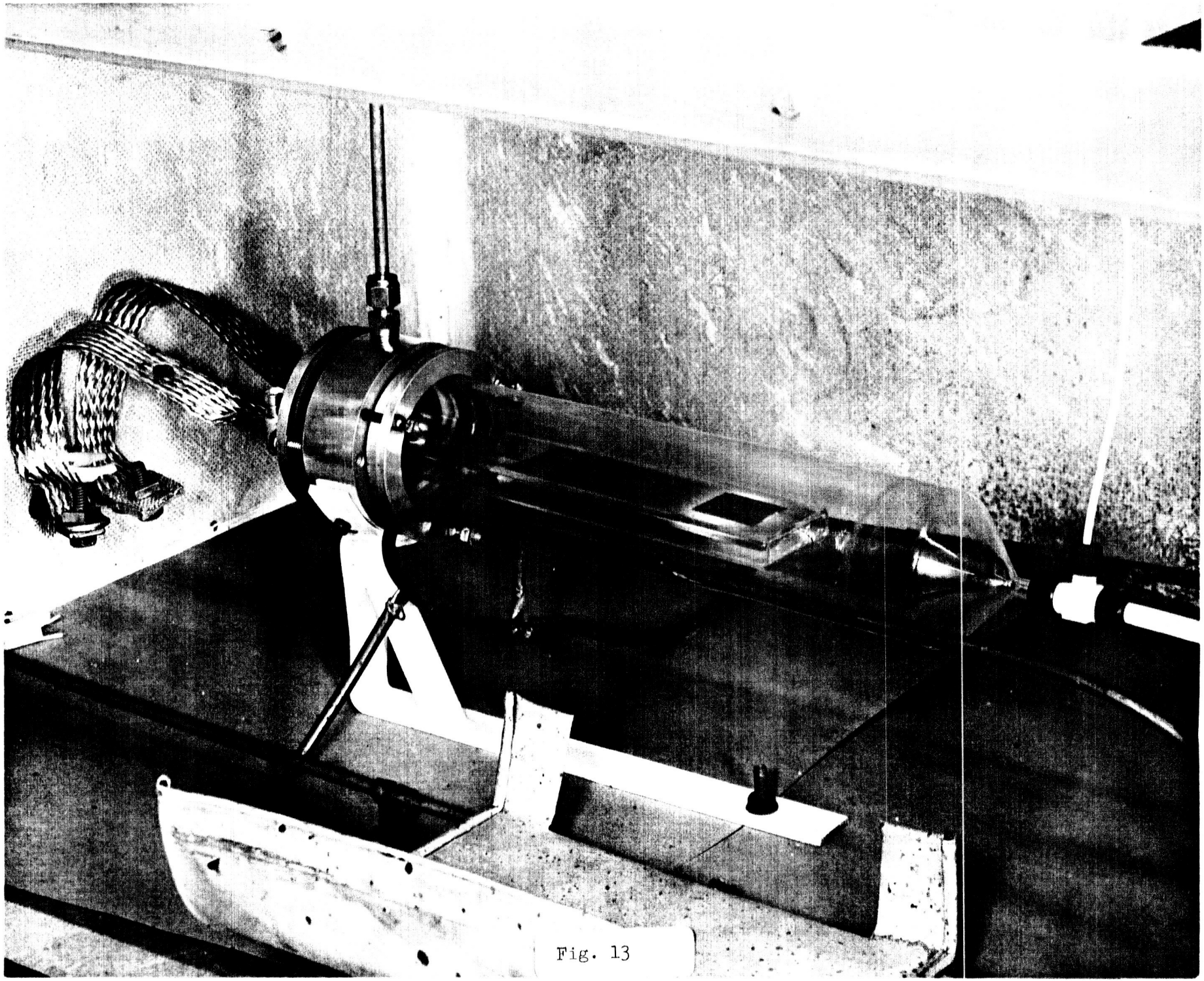

Fig. 13

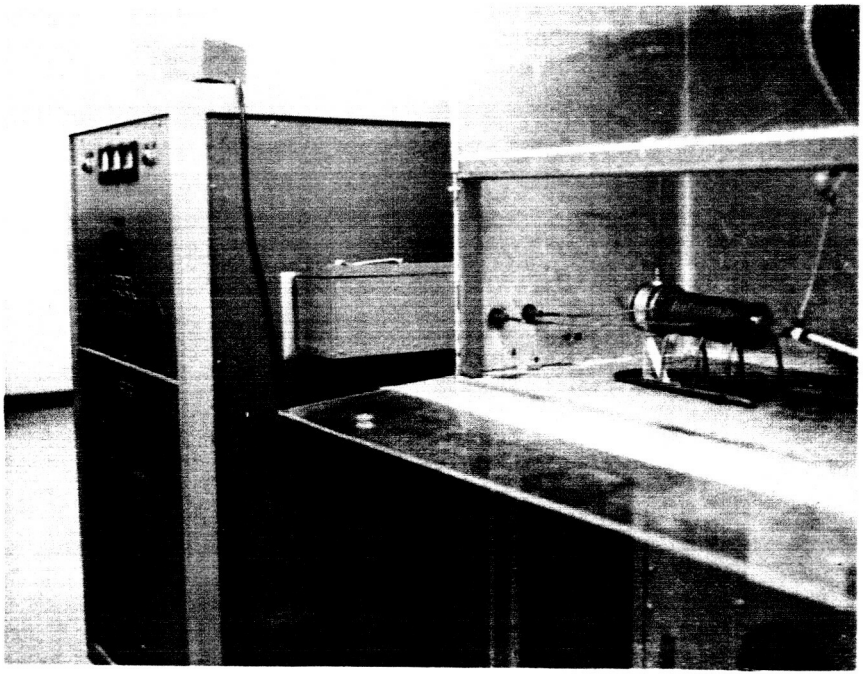

Fig. 14

the resistance heater was used because of the smaller heat zone and the use of a metal heat reflector which prevented silicon from depositing on the bottom of the heater sheath. Also, the majority of the runs done previously were of shorter duration.

It was also noticed that after deposition the slices which were placed directly on the quartz heater sheath surface were very brittle and were easily cracked. Figure 15 is a picture of the edge of one of these broken slices, the epitaxial layer being at the top of the photograph. It can be seen that the cleavage or slip planes are curved. Inspection of the surface of the mask material after deposition revealed a white crystalline formation which is believed to be devitrified quartz. It is quite likely that the combination of deposited silicon, devitrified quartz, and quartz itself induced strains into the substrate material during cooling due to the differences in coefficients of expansion. After evaluation of these problems, it was decided to eliminate the quartz sheath entirely and place the slices directly on a pure graphite block which would no longer be isolated from the $SiCl_4$ and H_2 atmosphere. The graphite block was supported by a quartz frame as shown in Fig. 16. Utilizing the RF generator, the temperature uniformity of the heater was checked using a Leeds and Northrup optical pyrometer and was found to be within 10°C over the 6 inch length at 1400°C, with no noticeable difference across the width of the heater. This represented an increase of about 200% of usable heat zone over that previously obtained with the resistance heater. The 12 inch long quartz reaction tube previously used was also replaced by a 19 inch long quartz tube. The additional 7 inch length of the tube results in a more uniform gas flow over the deposit area in the reactor and thus yields a more consistent epitaxial layer thickness.

The drift field cell design which Heliotek is using to produce drift field solar cells requires a highly doped, thick deposit. Therefore, work during the growth study period was directed to attain highly doped,

Fig. 15

x 50

thick deposits of 8 to 10 mils thickness. After the addition of the RF generator and the modification of the reactor several deposition runs were made. These runs revealed that the deposition rate had decreased to about 1μ/min due to the configuration of the new system.

The cross section in Fig. 17 is of a sample having an epitaxial layer 12 mils thick. The deposited layer is the upper half of the image. The deposition was made at 1075°C, using an $SiCl_4$ vapor pressure of 46 mm and a hydrogen gas flow of about 4 liters per minute. The duration of deposition was 200 minutes, thus yielding a growth rate of 1.5μ/min. In order to increase the deposition rate to the previous rates of 2 to 3μ/min, it was necessary to increase the vapor pressure of the $SiCl_4$ from 46 mm to 94 mm. This was accomplished by increasing the temperature of the bath in which the $SiCl_4$ flask is located. Along with this change in vapor pressure it was necessary to increase the hydrogen gas flow rate. A concentration of 3.2% of $SiCl_4$ in the hydrogen gas was required for a growth rate of 2.5μ/min in the modified reactor chamber. Therefore, in order to deposit the desired 10 mils of epitaxial material, runs of 100 minute duration are required. The cross section in Fig. 18 was made using the modified parameters. This sample had a deposited layer (left side of photo) of 9.5 mils thickness. The deposit was made at a temperature of 1200°C, a time duration of 120 minutes, a $SiCl_4$ vapor pressure of 94 mm, and a hydrogen flow of 20 liters per minute, thus yielding a growth rate of 2μ per minute. Both of the above samples (Figs. 17 and 18) were deposited using RF heating. The sample in Fig. 17 was made using the quartz heater sheath (Fig. 13), the sample in Fig. 18 was deposited using the bare carbon heater (Fig. 16).

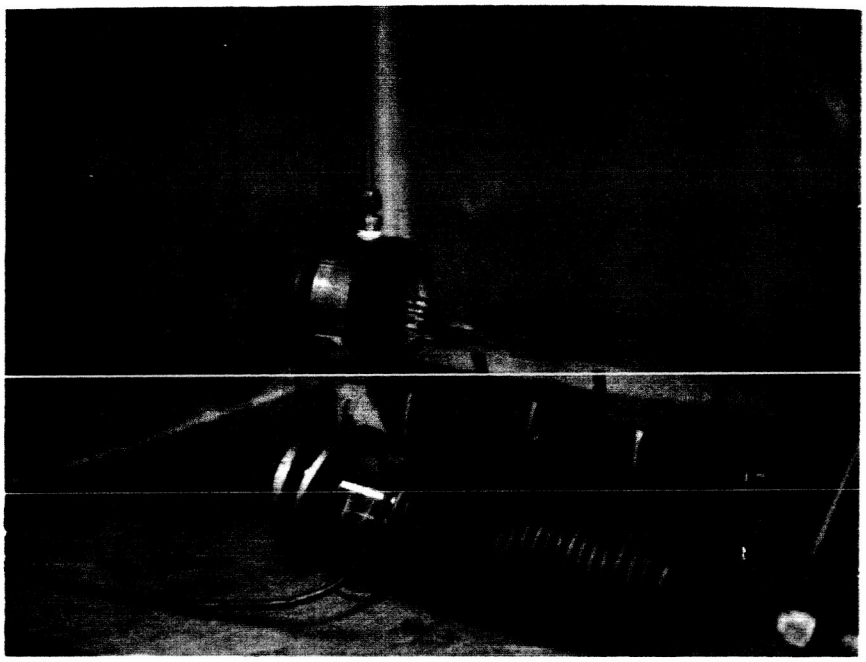

Fig. 16

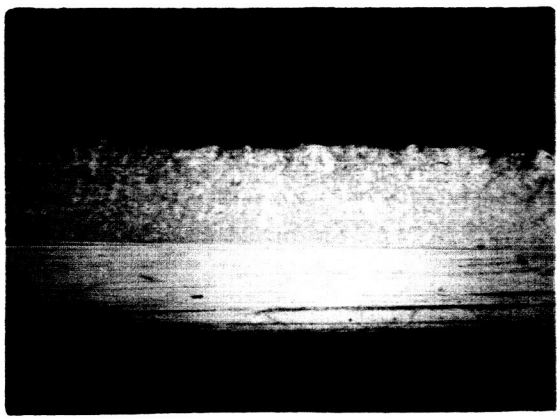

Fig. 17
x 50

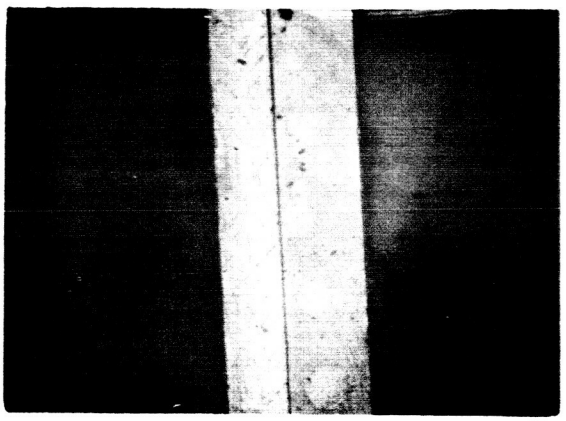

Fig. 18
x 50

During the second phase, a larger silicon tetrachloride reservoir was installed. This reservoir has a capacity of 1.5 liters. One of the primary reasons for the larger reservoir was that during the epitaxial run, the deposition rate was found to decrease with time when the smaller reservoir was utilized. This was attributed to the decreasing depth of liquid silicon tetrachloride through which the hydrogen gas is bubbled. When the depth of liquid silicon tetrachloride is deep enough in the reservoir so that the hydrogen gas bubbles reach a steady state condition for a given temperature, the mole ratio can be calculated. However, when this liquid level decreases below the point where the steady state prevails the bubbles do not saturate with $SiCl_4$ and the ultimate mole ratio decreases, resulting in a slower deposition rate.

The old $SiCl_4$ reservoir had a capacity of 500 mL of liquid and the change of depth was 1.375 inches/100 mL. The larger reservoir, having a greater diameter, gives a change of 0.55 inches /100 mL. The reservoir is equipped with three tubes. The gas inlet tube is fitted with a quartz frit which is used to disperse the incoming gas to small bubbles in the liquid $SiCl_4$. (Small bubbles saturate more rapidly than large bubbles due to the higher surface area to volume ratio in the former case.) The second tube is the gas outlet which leads to the reaction chamber. The last tube is used as a filler tube and is sealed by a removable Teflon fitting.

5.0 EVALUATION TECHNIQUE

Heliotek is presently using a potting and angle lap technique in order to evaluate epitaxial growths and diffusions. The angle lapping technique allows one to magnify the layers being investigated thus achieving more accurate measurements. First the thickness of the sample to be cross-sectioned is measured by means of a dial indicator or micrometer and recorded. Then the sample is encased in a cylindrical lucite block using a Buhler centiment press. The sample is placed in the lucite block at an angle. After the molding of the sample is completed, the lucite block is ground off until the sample is exposed as shown in Fig. 19. The silicon is then polished and stained. A copper staining method is used to define the epitaxial growth interface and/or junction.

Measurements of the cross section are made on a metallographic microscope equipped with a multidivision reticule. Most of the cross sections can be measured at 50 X magnification. The measurement A of Fig. 19 is the measurement (in mils) of the cross-sectioned sample before potting. The measurements B and C of Fig. 19 are measured by using the reticule in the microscope. Since the actual thickness A (in mils) is known and B and C are known in relative units, the distance X can be determined by simply using the ratio:

$$A(\text{mils})\,\frac{C}{B} = X(\text{mils}) \qquad \text{(Eq. 1)}$$

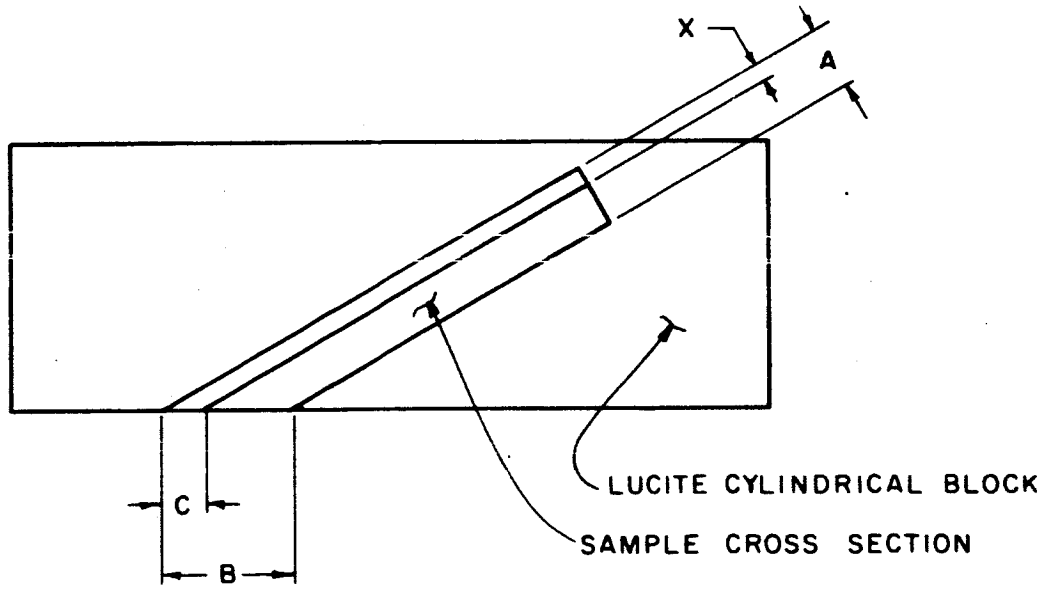

FIG. 19

T—2314

6.0 DIFFUSION TECHNIQUES

The drift field region is formed by the diffusion of impurities from the highly doped epitaxial layer (10^{19}atom/cm^3) into the substrate material (10^{15}atom/cm^3). The impurity gradient formed by the diffusion starts at the interface between the epitaxial layer and the substrate surface and extends into the substrate material. For maximum power output from a radiation resistant solar cell with a drift field region, Wolf[1] has calculated that an electrostatic potential difference of 0.118V and a field width of about 10^{-3}cm (about 0.4 mils) is needed.

The sample shown in the photo Fig. 20 is a cross section of a chip obtained from a slice after a 2 hour, 1250°C diffusion which was Step No. 4 of the fabrication process. A view of the cross section before staining is at right and after staining is at left. The unstained photo (right side) shows interference fringes which are displaced at the interface of the epitaxial layer (top) and the substrate (bottom). The stained photo (left) shows a dark band that starts at the interface and extends 0.7 mils into the substrate material. This dark band is caused by differential staining of the drift field region. Both sides of the photo were taken at the same spot and at the same magnification and show the correlation of the two methods for analyzing the structure.

The cross sections in Figs. 21 and 22 are chips taken from the edge of drift field cells H-2 and H-5 respectively. In both photos the gray band marked X delineates the diffused impurity gradient which is the base region drift field. The regions X in both photos are about 0.5 mils thick. This measurement agrees precisely with the theoretically predicted thickness, based on the diffusion time and temperature, and is the desired diffusion depth described in Step 4 of the Fabrication Process section. The interface between the epitaxial layer and the substrate material is at the bottom of region X and appears as a faint dark line. The epitaxial layers (Region B) extend from the bottom of

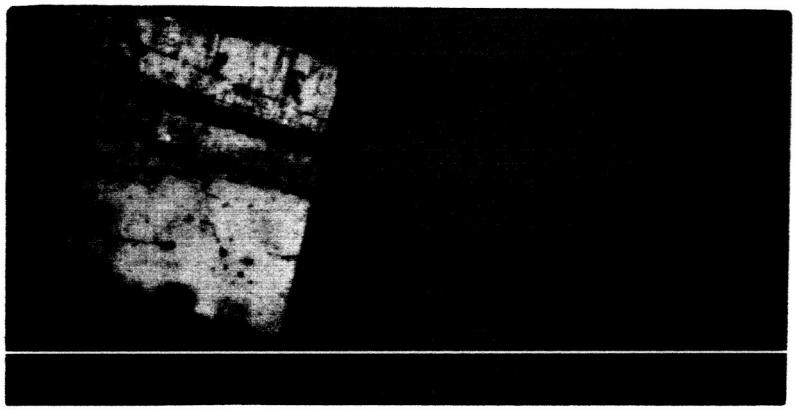

Fig. 20

x 65

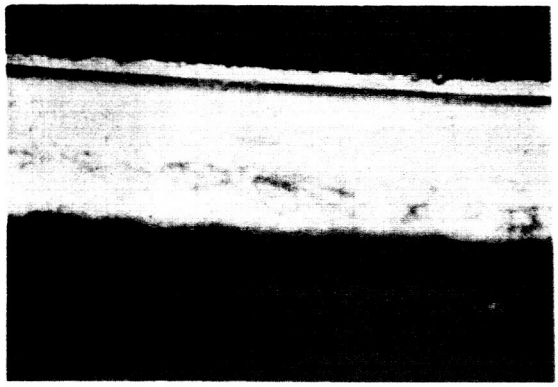

Fig. 21

50X

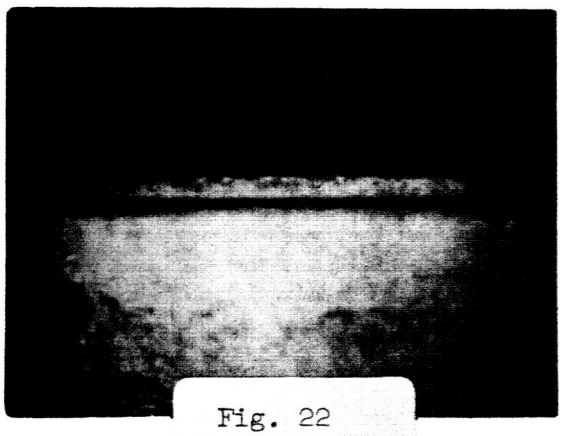

Fig. 22

50X

region X to the bottom or back side of the cell and have thicknesses of 7 mils in Photo 21 and 8 mils in Photo 22. The substrate material (Region A) starts at the top of the cell, where the N^+/P junction is located, and extends to the bottom of the region X. The cross-sectioned samples have substrates which were lapped and etched to thicknesses of 1.2 mils and 1.5 mils for Figs. 21 and 22 respectively. Since these first samples were made to test out the fabrication techniques it was decided that the total substrate thickness should be about 1.0 mils thick, instead of the theoretically optimum thickness of about 0.5 mils. This additional thickness was utilized as a safety factor to prevent the possibility of etching through the substrate material and into the epitaxial layer. It should be noted that for the maximum radiation resistance and cell performance after a 1 MeV electron flux of 10^{14} - $10^{16} e/cm^2$ the substrate should theoretically be about 12μ (0.47 mils) thick.

During the lapping and etching to remove the excess substrate material in Step No. 6 of the fabrication procedure, some cracking of the substrate was encountered. This problem of cracking has been attributed to strain between the substrate and the deposited layer which is probably due to a crystal lattice mismatch between the epitaxial layer and the substrate. In order to minimize the strain, the deposition temperature was raised from 1075°C to 1200°C, since it was found that more uniform single crystal deposits are made at 1200°C. This alleviated the problem of substrate cracking to some extent, however the substrate still has, on occasion, a tendency to crack during the last few mils of substrate removal.

In order to minimize or eliminate this breakage, attempts during the second phase were made to remove the excess substrate material by etching alone. By utilizing the etching method, Step 5 (plane parallel lapping of epitaxial layer) can be eliminated, and Step 7 (removal of excess substrate) may be simplified. An additional advantage would be that the process time is considerably shorter, thus adding to the economy of the process.

The first group of drift field solar cells produced during the second phase (these cells were being made to make up the third lot of samples since start of contract) were fabricated using the above modified process which required etching of the excess substrate away, and all these cells were found to be electrically shorted. Investigation of the surfaces of the cells revealed small pits and an uneven surface. The surface may be seen in Figure 23. The interference fringes indicate variations in the surface and show the depth of some of the pits, each fringe representing approximately 0.3μ. The etchant used for this group of cells was a solution of 5 parts Nitric, 1 part Hydrofluoric, 4.4 parts Acetic Acid saturated with Iodine.

The interference pattern on the surface of a drift field cell after etching in a solution of 2 parts Nitric acid, 1 part Hydrofluoric and 1 part Acetic acid is shown in Figure 24. It can be seen that the surface in Figure 23 is considerably more irregular than that of Figure 24 indicating that the 2:1:1 HNO_3: HF: CH_3COOH etch should provide better surfaces than the etch which was used in the fabrication of the first group of cells. The substrate thickness of the first group of cells produced by etching alone (no lapping) closely approached the theoretically optimum thickness of about 0.5 mils (12 microns). However the shorting problems mentioned above were encountered when the substrates were reduced to this thickness.

It is believed that the formation of the etch pits observed on the cell surfaces of the first group of samples was due to strains in the substrate material which propagated from the substrate-epitaxial interface. Since the etch pits occurred prior to formation of the p-n junction, this caused low resistance shunt paths which resulted in electrically shorted cells.

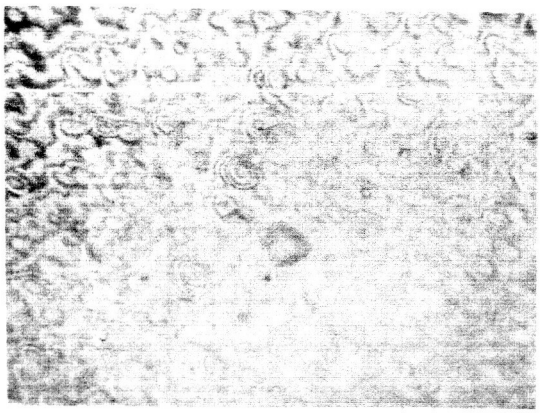

FIG.23

PHOTO NO. 1

65X

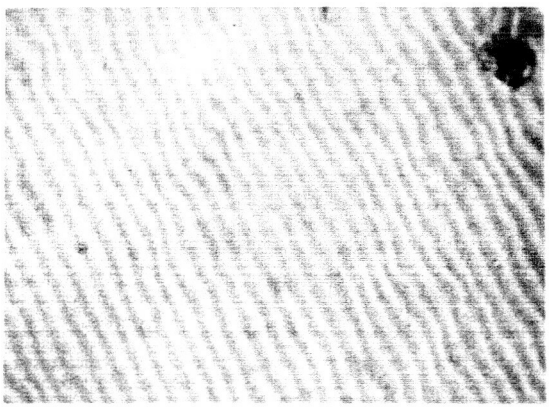

FIG.24

PHOTO NO. 2

65X

Also, due to the proximity of the p-n junction to the substrate-epitaxial interface, imperfections at this interface could give rise to non-uniform junction characteristics which further contributed to the failure of the cells to give significant power output.

In analyzing the shorted electrical characteristics of this group of cells, a number of mesas were etched on two of the cells. The diode characteristics were tested on each of the mesas and each mesa was classified, good, fair, or shorted. Schematic maps of the mesas were made and are presented in Figs. 25 and 26. The areas where good diode characteristics were found were usually encircled by fair diodes and gradually descend into the shorted diode area. This pattern is apparent in both samples considered.

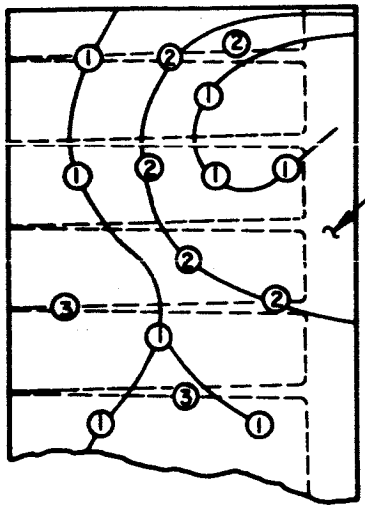

FIG. 25

DIODE CHARACTERISTICS

① FAIR

② SHORTED

③ GOOD

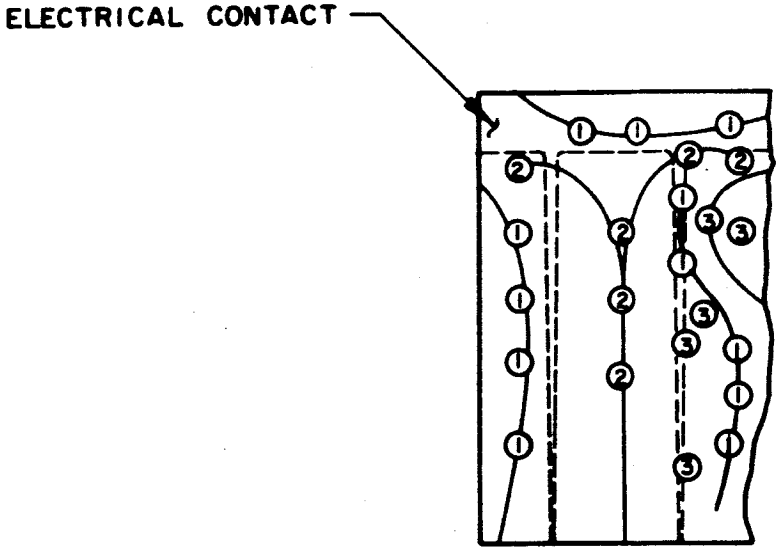

FIG. 26

IV. ELECTRICAL EVALUATION OF CELLS

The first lot of sample cells consisted of 6 drift field cells and 4 field free cells fabricated from the same ingots without the inclusion of a drift field to be used as control cells for electrical comparison before and after irradiation. Current voltage curves of all the sample cells were obtained under tungsten light having a color temperature of 2800°K. All measurements were made at a cell temperature of approximately 28°C. The results are summarized in Table I for the first 10 samples.

Spectral response measurements were also made on the basis of a light input which has a constant energy - wavelength relationship by means of the Heliotek filter wheel monochrometer system. The drift field cells showed peak responses at a wavelength of approximately 0.75 - 0.8μ, falling off on the long wavelength side to half peak output at a wavelength of about 0.95 - 1.0μ. The control cells from ingot E-3 showed a peak response at approximately 0.85Å while those from ingot E-4 showed peak response at 0.82μ. Considering the fact that all cells had the same junction depth, the data indicates that the minority carrier lifetime was somewhat lower for ingot E-4 than for E-3, since the E-3 control cells peaked at a longer wavelength, thus indicating that these cells have a greater response in the long wavelength region. These results are not surprising since ingot E-3 was of higher resistivity material, and the minority carrier lifetime typically increases with increasing material resistivity, other material parameters being identical. It should be emphasized here that in order to obtain a proper and correct evaluation of the effects of a drift field on the radiation resistive characteristics of solar cells, comparisons must be made with non-drift field cells fabricated from the same material since differences in base region resistivity and the resultant minority carrier lifetime can affect the radiation resistance of a cell to a great extent[3]. Bearing this in mind Heliotek has included among the cell samples, 2 cells fabricated

TABLE I

Cell No.	Ingot No.	Dimension (cm)	Active Cell Area (cm^2)	Standard Tungsten Light Source				Sunlight 100 mW/cm^2	
				I_{sc} (mA)	I_{sc}/cm^2 ($mA\text{-}cm^{-2}$)	V_{oc} (Volts)	Eff. %	I_{sc} (mA)	I_{sc}/cm^2 (mA/cm^2)
H-1	E-3	1 x 2	1.8	46.0	25.6	.48	8.9	49.5	27.5
H-2	E-3	1 x 1	.9	23.0	25.6	.51	9.2	24.8	27.5
H-3	E-3	1 x .4	.36	6.0	16.7	.43	4.7	8.0	22.2
H-4	E-4	1 x .5	.45	10.7	24.8	.54	9.5	12.4	27.6
H-5	E-4	1 x .5	.45	10.05	22.3	.51	8.4	11.2	24.9
H-6	E-4	1 x .5	.45	7.0	15.5	.475	5.3	8.1	18.1
H-7*	E-3	1 x 2	1.8	61.6	34.3	.387	6.2	57.0	31.6
H-8*	E-3	1 x 2	1.8	59.7	33.2	.370	4.9	55.5	31.4
H-9*	E-4	1 x 2	1.8	55.0	30.4	.537	11.9	55.6	31.5
H-10*	E-4	1 x 2	1.8	55.0	30.4	.545	12.8	55.6	31.5

*Cells fabricated without base region drift-field.

from each ingot which do not include a base region drift field so that their behaviour with respect to radiation damage can be compared with that obtained from the drift field cells.

It can be seen from Table I, that the efficiency of the control cells of ingot E-3 is quite low. This is due to the extremely high resistivity of the parent material which gives rise to high base region series resistance in the non-drift field cell having a base region thickness of about 20 mils, and to a higher metal-semiconductor contact resistance. In evaluating the radiation damage characteristics of these non-drift field cells one may want to consider only the light generated current parameter since this is relatively unaffected by the extremely high cell resistance. The cell can be back biased sufficiently to obtain this parameter if the slope of the current voltage curve is not normal to the current axis at zero voltage.

It can also be observed from the table that the short circuit current densities of the drift field cells are from 20 - 50% lower than those obtained from the respective control cells in tungsten light. In sunlight the difference between the short circuit current densities of the control cells and the drift field cells is reduced to between 13 - 43%. This is a consequence of the observation that the drift field cells have a higher blue to red response ratio than the control cells. The open circuit voltages of the E-3 drift field cells are considerably higher than those obtained for the E-3 control cells. This is probably due to the fact that the junction potential of the drift field cells is higher than that of the very high resistivity (greater than 200 ohm cm) control cells because, in the former case, the Fermi level near the junction has been modified by the inclusion of the drift field. That is to say, the drift field diffusion has resulted in a lowering of the substrate resistivity due to the additional impurities introduced. In the case of the E-4 cells the open circuit voltages of the control (nondrift field) cells were greater

than those of the drift field cells. The substrate material here, however, had a resistivity of about 10 ohm cm, so that the superposition of the the drift field carriers over the existing carriers would not be expected to result in a substantial increase in junction potential over that found in the original, undiffused material. The relatively poor long wavelength collection efficiency of the drift field cells evident in the spectral response data verify the expectation that the effective minority carrier lifetime is smaller than that obtained in the base region of the non-drift field cells. The lifetime affects the open circuit voltage according to the following equations:

$$V_{oc} = \frac{AkT}{q} \ln \frac{I_L}{I_o}$$

$$I_o = C \sqrt{T} \left(\sqrt{\frac{\mu_n}{\tau_n}} \frac{1}{P_p} + \sqrt{\frac{\mu_p}{\tau_p}} + \frac{1}{N_n} \right)$$

Where V_{oc} is the open circuit voltage and τ_n and τ_p are the minority carrier lifetimes in the P and N regions respectively. Thus the open circuit voltage is directly related to the natural logarithm of the square root of the minority carrier lifetime in the base region. It is possible that decreased lifetime is not the only reason for a decrease in open circuit voltage of the drift field cells. Outside of common effects such as surface or bulk shunts, anomalies in the band structure particularly near the substrate - epitaxial interface may also cause a lowering of the junction potential.

Current voltage curves, the second lot of sample cells (H-11 through H-20) were obtained under tungsten light having a filament color temperature of 2800°K. This lot consisted only of cells fabricated from ingot E-5, which had a resistivity of about 10 ohm centimeters. All measurements were made at a cell temperature of approximately 28°C. The results are summarized in Table II. Current voltage curves of these cells were also made in a Spectrosun Model D-1203, m = 0 Solar Simulator at a cell temperature of approximately 28°C. The results are summarized in Table III. Measurements in sunlight at the same cell temperatures were also performed, at Sylmar, California. The data corrected to correspond to 100 mW/cm^2 intensity is presented in Table III.

Once again it can be seen, through comparison of the current densities shown in Table II with those of Table III, that the current densities obtained for the drift field cells in sunlight are considerably higher than those obtained in tungsten light because the drift field cells have a higher blue to red response ratio than the standard cell which was used to calibrate the tungsten light system.

In the case of cells H-11 through H-20 the current densities obtained from the drift field cells compare quite favorably with the control cells (H-18 and H-19). The open circuit voltages of the drift field cells are lower than the control cells which agrees with the results obtained on ingot E-4 which was of approximately the same resistivity.

Spectral response measurements were made on the basis of a light input which has a constant energy - wavelength relationship by means of the

TABLE II

Cell No.	Ingot No.	Dimensions (cm)	Active Area cm^2	Standard Tungsten Light Source						
				I_{sc} (mA)	I_{sc}/cm^2 (mA/cm^2)	V_{oc} (volts)	I (P-max) (mA)	V (P-max) (volts)	P-max (mW/cm^2)	Eff. %
H-11	E-5	1 x 2	1.8	40.9	22.7	.522	37.0	.410	15.2	8.4
H-12	E-5	.5 x 2	.8	21.0	26.2	.520	19.3	.425	8.2	10.3
H-13	E-5	.5 x 1	.45	11.2	24.9	.510	10.0	.410	4.1	9.1
H-14	E-5	.5 x 1	.45	9.4	20.9	.523	8.5	.430	3.7	8.1
H-15	E-5	.3 x 1	.27	4.7	17.4	.450	3.9	.380	1.5	5.5
H-16	E-5	1 x 1	.9	20.6	22.8	.516	19.0	.410	7.8	8.7
H-17	E-5	1.2 x 1	1.08	20.8	19.3	.482	19.0	.390	7.4	6.7
H-18*	E-5	1 x 2	1.8	57.3	31.8	.559	53.4	.462	24.7	13.7
H-19*	E-5	1 x 2	1.8	57.8	32.1	.558	53.7	.464	24.9	13.8
H-20	E-5	1.7 x 7	1.02	24.5	24.0	.480	22.6	.380	8.59	8.4

*Cells fabricated without base region drift field

TABLE III

	Sunlight 100 mW/cm^2			Solar Simulator 140 mW/cm^2	
Cell No.	I_{sc} (mA)	I_{sc}/cm^2 (mA/cm^2)	Eff. %	I_{sc} (mA)	I_{sc}/cm^2 (mA/cm^2)
H-11	48.1	26.7	9.9	56.9	31.6
H-12	25.0	31.2	12.2	31.0	38.8
H-13	13.4	29.8	10.9	15.0	33.3
H-14	13.0	28.9	11.2	13.8	30.7
H-15	6.5	24.1	6.9	7.5	27.8
H-16	24.1	26.7	10.1	28.3	31.4
H-17	25.9	24.0	8.5	29.8	27.6
H-18*	55.1	30.6	13.2	64.8	36.0
H-19*	55.1	30.6	13.2	65.1	36.2
H-20	25.8	25.3	9.2	32.5	31.8

*Cells fabricated without base region drift field.

Heliotek filter wheel monochromator system. The drift field cells showed peak responses at a wavelength of approximately 0.75 - 0.8μ. The control cells from ingot E-5 showed a peak response at approximately 0.83μ.

The third lot of sample cells were processed in the normal manner as previously described with final substrate thicknesses of 25 to 30μ in order to obviate possible detrimental effects of the substrate-epitaxial interface. These cells had good electrical characteristics with the exception of cell H-24 which had a very low shunt resistance and hence poor efficiency (m=0 efficiency of 5.6%). Current voltage curves of all the sample cells were also obtained under tungsten light having a filament color temperature of 2800°K. All measurements were made at a cell temperature of approximately 28°C. The results are summarized in Table IV.

Complete current-voltage measurements were also made in a Spectrosun Model D-1203, m=0 Solar Simulator at a cell temperature of approximately 28°C. The results are summarized in Table V.

Spectral response measurements were made on the basis of a light input which has a constant energy-wavelength relationship, by means of the Heliotek filter wheel monochromator system. The drift field cells showed peak responses at a wavelength of approximately 0.75 to 0.8μ. The control cells from ingot E-6 showed a peak response at approximately 0.82μ.

The fourth lot of sample drift field cells submitted during the contract had substrate thicknesses of 16.5μ. The photograph presented in Fig. 26 is a cross sectioned chip taken at the center of one of the slices from which the drift field cells were fabricated. A cross section of the sample may be seen in Fig. 27, which shows the epitaxial material (B) on the right and the substrate (X) to the left. The epitaxial layer (region B) is 10.1 mils thick and the substrate (region X) is 12.3 mils. The drift field is the dark region in the area X, starting at the substrate-epitaxial layer interface (right end of region X) and extending to the left. The drift field region is 0.5 mils wide. The mechanical polishing operation of the substrate surface prior to the epitaxial

TABLE IV

Standard Tungsten Light Source

Cell No.	Ingot No.	Dimensions (cm)	Active Area cm^2	I_{sc} (mA)	I_{sc}/cm^2 (mA/cm^2)	V_{oc} (volts)	I (P-max) (mA)	V (P-max) (volts)	P-max (mW/cm^2)	Eff. %
H-21	E-6	1 x .55	.44	12.0	27.3	.530	11.0	.435	4.78	10.9
H-22	E-6	.8 x .5	.3	7.5	25.0	.480	7.6	.343	2.61	8.6
H-23	E-6	1 x1	.8	21.0	26.3	.520	18.7	.418	7.82	9.7
H-24	E-6	1 x1	.8	21.3	26.6	.460	14.7	.325	4.78	6.0
H-25	E-6	1.2 x .8	.7	18.5	26.4	.485	15.2	.368	5.59	8.0
H-26	E-6	1 x .5	.4	10.2	25.5	.511	9.3	.420	3.90	9.7
H-27	E-6	1 x .5	.4	11.0	27.5	.523	10.1	.411	4.15	10.4
H-28	E-6	.8 x .4	.24	7.0	29.2	.523	7.0	.374	2.61	10.8
*H-29	E-6	1 x 2	1.8	59.0	32.8	.552	54.5	.46	25.	13.6
*H-30	E-6	1 x 2	1.8	59.0	32.8	.547	54	.43	23.2	12.8

*Cells fabricated without base region drift field.

TABLE V

SOLAR SIMULATOR

140 mW/cm^2

Cell Number	I_{sc} (mA)	I_{sc}/cm^2 (mA/cm^2)	Efficiency %
H-21	14.5	33.0	9.7
H-22	9.8	32.7	7.1
H-23	27.7	34.6	8.5
H-24	27.0	33.8	5.6
H-25	24.3	34.7	7.5
H-26	12.4	31.0	8.6
H-27	12.6	31.5	8.9
H-28	8.8	36.7	9.8
*H-29	65.5	36.9	11.0
*H-30	64.0	35.5	9.7

*Cells fabricated without base region drift field.

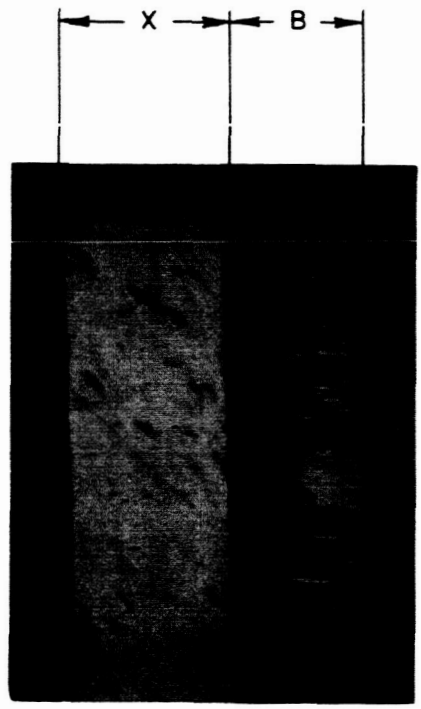

FIG. 27

MAGNIFICATION 100X

deposit was eliminated in the processing of these cells and a chemical polish etch technique was adopted. This was done to help minimize the strain and imperfections formed at the substrate-epitaxial interface, since it has been reported that epitaxial layers deposited on chemically etched surfaces show less crystalline imperfections than those deposited on mechanically polished surfaces[4] due to the minimization of surface crystalline damage in the former case.

The preparation of the substrate prior to epitaxial deposition for these cells was as follows: The substrate slice was lapped plane parallel to a thickness of 8 mils. The slice was then cleaned and etched. The etchant used was a two part Nitric, one part Hydrofluoric and one part Acetic acid solution, and the etching was performed in a tilted, rotating container, which supplied the necessary agitation to produce a uniform polish etch. Two mils of silicon were removed from each surface (4.0 mils from the total slice thickness) leaving a substrate slice of 4 mils thickness.

After epitaxial deposition and the drift field diffusion operation, the substrate thickness was further reduced. By using the thinner substrates, about 0.5 mils is removed by lapping and 3.0 mils by etching as compared to a removal of 5.5 mils by lapping and 3.0 mils by etching which is required with the thicker substrates. The lapping was done in order to remove a carbon black mask on the surface and any possible undergrowth, which would interfere with the etch and result in a non-uniform surface finish. The etching operation was performed in the etchant solution and the rotating, tilted container described above. By using the thinner, chemically polished substrates, the total fabrication time required to produce a drift field cell was also reduced.

---

4) G. A. Lang and T. Stavish, "Chemical Polishing of Silicon with Anhydrous Hydrogen Chloride", RCA Review, December, 1963.

During the electrical testing of some of the drift field cells, the electrical contacts of one cell peeled away from the silicon. The cell was subsequently stripped of all surface metals, and new contacts were evaporated and sintered in an effort to obtain a usable cell. In retesting the cell it was found the electrical output had degraded considerably as can be seen from Fig. 28. This cell was consequently withheld from the sample shipment and no further attempts were made to reclaim cells with damaged contacts. Current voltage curves of all the sample cells from this group were obtained under tungsten light having a filament color temperature of 2800°K. All measurements were made at a cell temperature of approximately 28°C. The results are summarized in Table VI.

The curves obtained from this series of sample cells exhibited a relatively poor shape and further analysis was made to determine the reason for this. The series resistances were found to be in the normally expected range of 0.4 ohms. Dark reverse currents were utilized to obtain a measure of the cell shunt resistance. The dark reverse diode currents were measured by reverse biasing the junction of the cell at 0.7 volts and measuring the current flow. This can be related to the cell shunt resistance through Ohm's law:

$$R_{shunt} = \frac{V}{I_{shunt}}$$

High efficiency cells usually have low dark reverse currents of the order of 10 μA, however high efficiency cells can still be obtained with dark reverse currents as high as 100 to 200 μA. Although cells H-35 and H-36 had very high shunt currents, it can be seen that cells H-31, 32, 33, 34, and 38 did not have high enough shunt currents to cause the very poor curve shapes which were observed.

It is well known that high values for the "A factor" in the diode equation will give rise to curve shapes similar to those observed for

TABLE VI

STANDARD TUNGSTEN LIGHT SOURCE

Cell No.	Ingot No.	Dim. (cm)	Active Area (cm^2)	I_{sc} (mA)	Dark Diode Rev. Char. (μA)	I_{sc}/cm^2 (mA/cm^2)	V_{oc} (Volts)	I (P-max) (mA)	V (P-max) Volts	(P-max) (mW)	Eff. %
H-31	E-6	1x1	0.9	17.3	23	19.23	0.47	14.75	0.347	5.12	5.7
H-32	E-6	1x1	0.9	18.5	13	20.55	0.49	16.0	0.363	5.81	6.45
H-33	E-6	1.2x1	1.08	23.2	80	21.5	0.43	19.8	0.312	6.18	5.72
H-34	E-6	2x0.9	1.6	40.0	80	25.0	0.44	34.3	0.328	11.25	7.04
H-35	E-6	1x1	0.9	21.2	>1000	23.6	0.44	17.6	0.316	5.57	6.18
H-36	E-6	1x0.8	0.7	17.0	>1000	24.3	0.50	13.8	0.378	5.22	7.45
H-37	E-6	1x1	0.9	25.0	50	27.8	0.51	22.2	0.385	8.55	9.5
*H-38	E-6	1x2	1.80	59.0	2	25.2	0.50	55.0	0.455	25.0	14.0
*H-39	E-6	1x2	1.8	58.3	9	32.5	0.54	54.0	0.445	24.1	13.4
*H-40	E-6	1x2	1.8	59.0	6	32.7	0.545	56.5	0.43	24.3	13.5

*Cell fabricated without base region drift field.

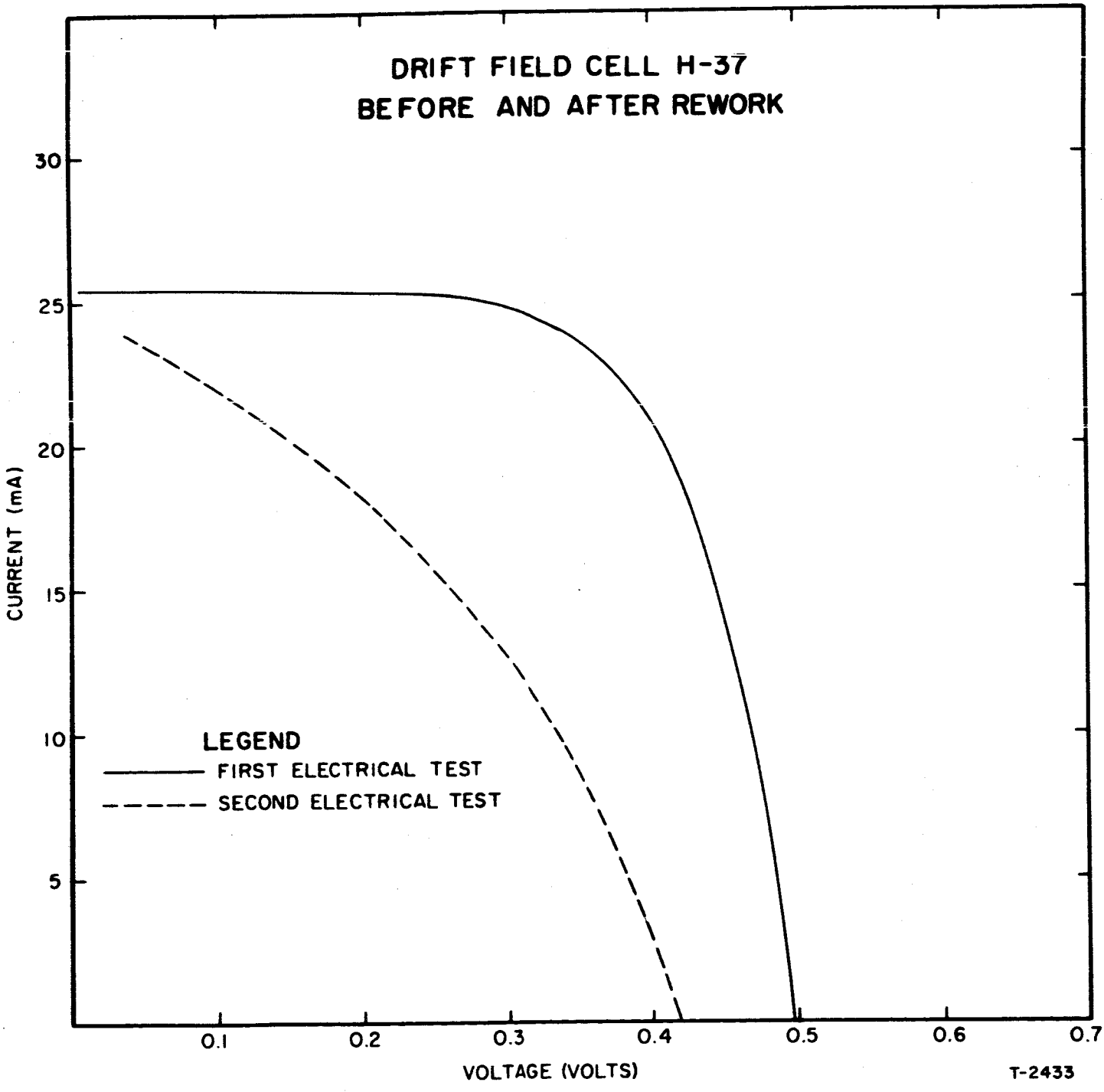
DRIFT FIELD CELL H-37
BEFORE AND AFTER REWORK
CURRENT (mA)
30
25
20
15
10
5
LEGEND
FIRST ELECTRICAL TEST
SECOND ELECTRICAL TEST
0.1
0.2
0.3
0.4
0.5
0.6
0.7
VOLTAGE (VOLTS)
T-2433

FIG. 28

the drift field cells. The A factor can be adversely affected by high dislocation and/or imperfection densities in regions near the junction and these dislocations and imperfections, in turn, can be caused by the epitaxial process since the junction is less than 20μ from the substrate-epitaxial interface. This possible cause of the observed curve shape will be further explored in Section V of this report.

Complete current-voltage measurements were also made on these sample cells in a Spectrosun Solar Simulator at a cell temperature of approximately 28°C. The results are summarized in Table VII.

Spectral response measurements were made on an equal energy light input basis as a function of wavelength by means of the Heliotek filter wheel monochromator system. The drift field cells showed peak responses at a wavelength of approximately 0.75 to 0.8μ as in the previous groups of samples. The control cells from ingot E-6 showed a peak response at approximately 0.82μ. These responses agree with those obtained on previous samples indicating that the spectral characteristics were quite consistent from lot to lot. Also, the percentage drops of efficiency in the m=0 Spectrosun system (as compared with the tungsten efficiencies) are similar to those obtained previously, thus giving further evidence of the consistency of the spectral characteristics.

TABLE VII

SOLAR SIMULATOR

140 mW/cm^2

Cell Number	I_{sc} (mA)	I_{sc}/cm^2 mA/cm^2	Efficiency %
H-31	19.5	21.7	4.65
H-32	21.5	23.9	5.42
H-33	25.0	23.2	4.43
H-34	47.0	29.4	5.91
H-35	25.4	28.2	5.46
H-36	20.6	29.4	6.58
H-37	30.0	33.4	8.25
* H-38	65.5	36.4	10.6
* H-39	65.0	36.0	10.4
* H-40	66.0	36.7	10.6

*Cells fabricated without base region drift field.

During the ninth month of the contract the epitaxial system was disassembled, cleaned and purged. Some difficulties were experienced subsequent to this, especially with growth rates. As a result, only enough usable epitaxial slices were deposited to allow the fabrication of three drift field cells.

Current voltage curves of these samples (fifth lot) were obtained under tungsten light having a filament color temperature of 2800°K, and cell temperature at 28°C. The electrical test data is presented in Table VIII.

Complete current-voltage measurements were also made on these sample cells in a Spectrosun Solar Simulator at a cell temperature of approximately 28°C. The results are summarized in Table IX.

Spectral response measurements indicated typical drift field cell spectral characteristics as observed previously.

In order to utilize all the active deposition area of the epitaxial heater, slices 1 x 6 inches (17 mils thick) were used in four epitaxial runs. Deposit times of 100 and 120 minutes were used. These deposition times usually result in 10 and 12 mil deposited layer thickness on (2) circular slices having a diameter of about 1-1/2 inches. However, using the large rectangular cells, the deposits were found to be only 5 and 6 mils thick. These thin deposits on the large area slices indicated that by increasing the silicon substrate area the deposition rate decreased. In performing these runs the mole ratio, temperature and vapor pressure of the $SiCL_4$ were held to the same values as in a normal run. An advantage of using the 1 x 6 inch substrates would be that more larger area cells could be obtained from one epitaxial run. However, since process modifications would obviously be necessary in order to use this approach, further investigations were postponed, and work with the more familiar circular slices was continued.

TABLE VIII

STANDARD TUNGSTEN LIGHT SOURCE
100 mW/cm^2

Cell No.	Ingot No.	Dim. (cm)	Active Area (cm^2)	I_{sc} (mA)	I_{sc}/cm^2 (mA/cm^2)	V_{oc} (Volts)	I (P-max) (mA)	V (P-max) Volts	(P-max) (mW)	Eff. %
H-41	E-7	.9 x .9	.72	18.0	25.0	.555	16.3	.450	7.34	10.2
H-42	E-7	1 x1.5	1.35	31.6	23.4	.542	27.8	.420	11.68	8.6
H-43	E-7	1 x .7	.6	14.4	24.0	.537	12.0	.420	5.04	8.4
*H-44	E-7	1 x 2	1.8	59.2	32.9	.550	55.0	.452	24.86	13.8

*Cell fabricated without base region drift field.

TABLE II

Cell No.	Solar Simulator 140 mW/cm^2 I_{sc} (mA)	I_{sc}/cm^2 (mA/cm^2)	Eff. %
H-41	23.0	31.9	9.4
H-42	40.8	30.2	8.1
H-43	19.8	33.0	8.7
*H-44	63.9	35.5	10.8

The electrical characteristics of the sixth lot of sample cells in tungsten and solar simulator systems are presented in Tables X and XI.

In the course of the drift field cell fabrication it was notices that the substrate slices were sometimes bowed. This warpage was attributed to the rapid increase and decrease of temperature at the beginning and end of the epitaxial deposition step. In order to verify this finding, two 20 minute epitaxial runs were performed. These deposits were made on 4 to 5 mil substrate slices. The temperature of the first epitaxial run was increased and decreased rapidly, and the slices were warped to the extent that when flexed, an oilcanning effect was noticed. The temperature of the second run was increased and decreased gradually and the resulting deposited slices showed only minor bowing. It was subsequently found, however, that even this slight bowing could be detrimental since some sections of the resultant cells were lapped thinner than others and it was subsequently found that these sections etched through to the epitaxial layer as a result of the pre-diffusion etch. Five cells of the seventh lot of cells were made unusable because of this problem.

A minimum amount of bowing was finally achieved through careful temperature adjustments in the pre and post deposition cycles which minimized thermal strain. Six of the seven sample drift field cells submitted in the seventh lot were fabricated from slices heat treated in this manner. A new ingot was utilized (Ingot E-10) as substrate material for these latter depositions and a number of control cells indicated that the material was reasonably good, yielding non-drift field cells of 12 to 13% tungsten efficiency. Because of the slight bowing and the observation that the substrate removal etch did not seem to be uniform enough in etch rate to provide the close control necessary to circumvent the effects of the bowing, the final substrate removal was performed by a lapping operation similar to that used during Phase I. Also, there was a return to use of thicker substrates.

TABLE X

STANDARD TUNGSTEN LIGHT SOURCE
100 mW/cm^2

Cell No.	Ingot No.	Dim. (cm)	Active Area (cm^2)	I_{sc} (mA)	I_{sc}/cm^2 (mA/cm^2)	V_{oc} (Volts)	I (P-max) (mA)	V (P-max) Volts	(P-max) (mW)	Eff. %
H-45	E-6	1.4 x 0.8	1.04	21.8	22.2	.560	19.7	.452	8.90	9.1
H-46	E-6	1.0 x 1.2	1.08	23.0	21.3	.518	20.5	.418	8.57	7.9
H-47	E-6	1.7 x 0.9	1.44	35.0	24.3	.535	31.5	.427	13.45	9.4
H-48	E-6	1.5 x 0.6	.84	22.9	27.3	.535	20.0	.414	8.28	9.9
H-49	E-6	1.0 x 2.0	1.90	43.5	24.2	.535	38.9	.417	16.22	8.5
H-50	E-6	1.0 x 2.0	1.90	39.5	21.9	.533	32.2	.410	13.20	6.9
H-51	E-6	1.2 x 0.7	.84	29.0	34.9	.528	25.6	.430	11.01	13.2
*H-52	E-6	1.0 x 2.0	1.80	61.7	34.3	.551	56.0	.404	22.62	12.6
*H-53	E-6	1.0 x 2.0	1.80	60.1	33.4	.551	55.0	.420	23.10	12.8
H-54	E-6	1.0 x 2.0	1.90	39.5	20.8	.516	32.2	.360	11.59	6.1

*Cell fabricated without base region drift field.

TABLE XI

Solar Simulator
140 mW/cm^2

Cell No.	I_{sc} (mA)	I_{sc}/cm^2 (mA/cm^2)	Eff. %
H-45	30.0	30.6	8.2
H-46	30.3	28.1	6.8
H-47	44.5	30.9	6.5
H-48	27.2	32.4	8.6
H-49	56.5	29.7	7.1
H-50	53.6	28.2	6.8
H-51	35.8	42.5	11.7
*H-52	66.5	36.9	9.5
*H-53	65.9	36.6	9.7
H-54	54.6	28.7	5.9

Five drift field cells were also fabricated from lower resistivity material (1 ohm-cm) to determine the electrical characteristics of these cells. These cells have been submitted to NASA for possible radiation experiments to compare the radiation tolerance of these drift field cells with the higher resistivity drift field cells. These low resistivity drift field cells were not, however, counted among the sample cells and were submitted in addition to the contract requirements, since they do not constitute the best theoretical design.

Current voltage curves of all the sample cells of Lot 7, Phase II as well as those fabricated from 1 ohm-cm material, were obtained under tungsten light having a filament color temperature of 2800°K and Spectrosun m=0 solar simulator. All measurements were made at a cell

temperature of approximately 28°C. The results are summarized in Tables XII and XIII The solar simulator current densities of the high resistivity ("H" numbered) drift field cells of this lot closely approach that of the field free control cells and are lower by only 3 to 15%, with the average current degradation being only 9%. The simulator efficiencies of the drift field cells are on the average 18% lower than those of the field-free control cells, the additional degradation being due to a lower average maximum power voltage for the drift field cells superimposed upon the lower maximum power current. It can be seen, however, that the tungsten open circuit voltage of drift field cell H-55 is identical to one of the control cells (H-62) and only .002 volts lower than the other two control cells, indicating that the lower V_{oc} of the drift field cells may not be inherent in the cell design, but rather due to processing variables.

The low resistivity drift field cells are designated in the two tables with "X" prefixes to note that these are not contractual sample cells. These cells are seen to have higher open circuit voltages and lower short circuit currents than the high resistivity drift field cells. Also, the efficiencies of the low resistivity drift field cells seem to be slightly higher than those of the high resistivity cells.

Current voltage curves of all samples submitted as Lot 8 of Phase II were obtained in tungsten and m=0 simulator systems under standard test conditions. The electrical test data are presented in Tables XIV and XV respectively.

The efficiencies of the drift field cells were found to be quite consistent for this lot of cells indicating good processing control. Extreme care was taken in the fabrication of these cells to insure that the substrate material was not etched or lapped through to the epitaxial material. This was required since a slight amount of bowing was still

evident in the epitaxial slices from which the cells were fabricated, although the bowing was not nearly as severe as had been observed in the previous lots.

The drift field cells showed efficiency degradations of between 10 and 15 percent in going from tungsten to solar simulator light systems, while the field free cells showed degradations of about 20 percent under the same conditions. This is similar to figures obtained on previous drift field cells. (See for example, monthly Report No. 8 and Section V of this report.)

The spectral response characteristics were also representative of those normally obtained for drift field cells and exhibited response at wavelengths between 0.75 and 0.8 microns.

TABLE XII

100 mW/cm² Standard Tungsten Light Source

Cell No.	Ingot No.	Dim. (cm)	Active Area (cm^2)	I_{sc} (mA)	I_{sc}/cm^2 (mA/cm^2)	V_{oc} (Volts)	I (P-max) (mA)	V (P-max) (Volts)	(P-max) (mW)	Eff. %
H-55	E-10	1 x 1	.9	20.0	22.1	.538	17.7	.457	8.09	9.0
H-56	E-10	1 x 2	1.8	40.1	22.1	.504	34.5	.393	13.56	7.5
H-57	E-10	1 x 1	.9	22.8	25.3	.502	19.8	.398	7.89	8.8
H-58	E-10	1 x 1	.9	23.0	25.5	.498	19.6	.402	7.88	8.7
H-59	E-10	1 x 2	1.8	43.5	24.2	.531	38.5	.425	16.35	9.1
H-60	E-10	1 x 2	1.8	44.7	24.8	.508	40.0	.402	16.10	8.95
H-61	E-10	1 x 2	1.8	46.2	25.6	.501	41.0	.398	16.31	9.05
*H-62	E-10	1 x 2	1.8	52.8	29.3	.538	49.2	.443	21.8	12.1
*H-63	E-10	1 x 2	1.8	53.8	30.0	.540	49.9	.440	22.0	12.2
*H-64	E-10	1 x 2	1.8	52.2	29.0	.540	49.0	.440	21.6	12.0
** X-1	E-8	1 x 2	1.8	44.2	24.6	.570	40.5	.467	18.7	10.4
** X-2	E-8	1 x 2	1.8	44.0	24.5	.578	39.2	.480	18.7	10.4
** X-3	E-8	1 x 2	1.8	41.3	23.0	.573	38.0	.478	18.4	10.1
** X-4	E-8	1 x 2	1.8	40.1	22.3	.585	36.0	.430	15.45	8.6
** X-5	E-8	1 x 2	1.8	42.5	23.6	.568	36.0	.467	16.75	9.3
** *X-6	E-8	1 x 2	1.8	53.0	29.4	.580	47.5	.485	23.0	12.75

*Cell fabricated without base region drift field.

**Experimental cells fabricated from 1 ohm-cm resistivity substrate material.

TABLE XIII

Solar Simulator 140 mW/cm²

Cell No.	Ingot No.	Dim. (cm)	Area (cm²)	I_{sc} (mA)	I_{sc}/cm^2 (mA/cm²)	Eff. %
H-55	E-10	1 x 1	.9	26.2	29.1	8.60
H-56	E-10	1 x 2	1.8	52.3	29.1	7.20
H-57	E-10	1 x 1	.9	28.7	31.9	8.15
H-58	E-10	1 x 1	.9	29.5	32.8	8.40
H-59	E-10	1 x 2	1.8	53.8	29.4	7.90
H-60	E-10	1 x 2	1.8	56.0	31.1	8.25
H-61	E-10	1 x 2	1.8	57.1	31.7	8.25
*H-62	E-10	1 x 2	1.8	60.3	33.5	10.10
*H-63	E-10	1 x 2	1.8	61.8	34.3	10.00
*H-64	E-10	1 x 2	1.8	59.9	33.3	9.70
** X-1	E-8	1 x 2	1.8	53.8	29.9	9.30
** X-2	E-8	1 x 2	1.8	53.1	29.5	8.60
** X-3	E-8	1 x 2	1.8	51.2	28.4	8.85
** X-4	E-8	1 x 2	1.8	50.8	28.2	8.17
** X-5	E-8	1 x 2	1.8	51.0	28.3	8.04
** *X-6	E-8	1 x 2	1.8	59.8	33.2	10.32

*Cell fabricated without base region drift field.

**Experimental cells fabricated from 1 ohm-cm resistivity substrate material.

TABLE XIV

100 mW/cm² Standard Tungsten Light Source

Cell No.	Ingot No.	Dim. (cm²)	Active Area (cm^2)	I_{sc} (mA)	I_{sc}/cm^2 (mA/cm^2)	V_{oc} (Volts)	I (P-max) (mA)	V (P-max) (Volts)	(P-max) (mW)	Eff. %
H-65	E-10	1 x 2	1.8	42.0	23.3	.561	37.6	.455	17.0	9.45
H-66	E-10	1 x 2	1.8	39.8	22.1	.530	31.1	.418	12.8	7.15
H-67	E-10	1 x 2	1.8	39.6	22.0	.552	35.7	.441	15.6	8.65
H-68	E-10	1 x 2	1.8	37.4	20.8	.548	33.6	.443	14.8	8.60
H-69	E-10	1.x 2	1.8	41.5	23.0	.531	35.0	.398	14.0	7.80
H-70	E-10	1 x 2	1.8	37.7	20.9	.542	33.5	.428	14.2	7.90
H-71	E-10	1 x 1	.9	21.2	23.6	.547	17.6	.458	8.05	8.95
H-72	E-10	1 x 1	.9	20.3	22.6	.540	16.8	.450	8.00	8.90
* H-73	E-10	1 x 2	1.8	53.8	29.9	.544	49.3	.443	21.60	12.00
* H-74	E-10	1 x 2	1.8	54.2	30.1	.547	49.7	.450	22.30	12.40

*Cell fabricated without base region drift field.

TABLE XV

Solar Simulator 140 mW/cm^2

Cell No.	Ingot No.	Dim. (cm)	Area (cm^2)	I_{sc} (mA)	I_{sc}/cm^2 (mA/cm^2)	Eff. %
H-65	E-10	1 x 2	1.8	50.2	27.9	8.1
H-66	E-10	1 x 2	1.8	48.2	26.8	6.8
H-67	E-10	1 x 2	1.8	48.9	27.1	8.0
H-68	E-10	1 x 2	1.8	47.9	26.6	7.7
H-69	E-10	1 x 2	1.8	51.0	28.3	7.0
H-70	E-10	1 x 2	1.8	46.5	25.8	7.15
H-71	E-10	1 x 1	0.9	25.5	28.3	8.05
H-72	E-10	1 x 1	0.9	25.0	27.8	7.78
* H-73	E-10	1 x 2	1.8	60.0	33.3	9.80
* H-74	E-10	1 x 2	1.8	60.9	33.8	10.00

*Cell fabricated without base region drift field.

Current voltage curves of all sample cells submitted as lot 9 were obtained in both tungsten and solar simulator light systems. The results are summarized in Tables XVI and XVII respectively. It can be seen that cells H-75 through H-78 have open circuit voltages about 30 to 40 mV lower than the field-free control cells H-83 and H-84. Further electrical evaluation showed these drift field cells to have normal shunt and series resistances which would not give rise to the low V_{oc} values observed. It was found that control cells which were phosphorus diffused at the same time as drift field cells H-75 through H-78 exhibited a 40 to 50 mV decrease in V_{oc} over that normally obtained from cells made from this control ingot and hence it is believed that the low V_{oc} of drift field cells H-75 through H-78 was a result of factors such as impurities present

when the p-n junction diffusion was performed. Drift field cells H-79 through H-82 were phosphorus diffused on a different occasion and all these cells had open circuit voltages which were from 9 to 26 mV higher than the field free control cells fabricated from the same starting material. Therefore, in this case the diffusion of the impurities to form the electrical junction was not deleterious to the open circuit voltage. The higher open circuit voltage indicates that the drift field is quite close to the electrical junction (see discussion of open circuit voltage in Second Phase Report).

Spectral response measurements made on the sample cells showed that the drift field cell responses peak in the 0.75 to 0.80 micron wavelength region, and the field free control cells peak in the 0.84 to 0.85 wavelength region. This indicates less red response in the drift field cells which can be attributed to decreased lifetime or the decrease in collection of carriers due to the proximity of the drift field to the junction.

TABLE XVI

STANDARD TUNGSTEN LIGHT SOURCE

100 mW/cm^2

Cell No.	Ingot No.	Dim. (cm)	Active Area (cm^2)	I_{sc} (mA)	I_{sc}/cm^2 (mA/cm^2)	V_{oc} (Volts)	$I_{P_{max}}$ (mA)	$V_{P_{max}}$ (Volts)	P_{max} (mW)	Eff. (%)
H-75	E-11	1x2	1.80	32.4	18.0	.502	29.4	.405	11.90	6.57
H-76	E-11	.9x1.9	1.44	34.2	23.8	.510	31.0	.410	12.70	8.82
H-77	E-11	1x1	.90	18.0	20.0	.513	16.0	.420	6.72	7.48
H-78	E-11	1x1	.90	17.6	19.6	.499	16.0	.390	6.25	6.95
H-79	E-11	1x2	1.80	33.7	18.7	.566	30.8	.469	14.45	8.05
H-80	E-11	1x1	.90	17.9	19.9	.599	16.0	.459	7.35	8.17
H-81	E-11	1x1	.90	15.7	17.5	.552	13.7	.452	6.20	6.90
H-82	E-11	1x1	.90	16.0	17.8	.559	14.3	.459	6.57	7.30
*H-83	E-11	1x2	1.80	61.0	33.9	.540	55.8	.433	24.10	13.40
*H-84	E-11	1x2	1.80	59.6	33.1	.543	55.8	.432	24.10	13.40

*Cell fabricated without base region drift field.

TABLE XVII

SOLAR SIMULATOR 140 mW/cm^2

Cell No.	Ingot No.	Dim. (cm)	Area (cm^2)	I_{sc} (mA)	I_{sc}/cm^2 (mA/cm^2)	Eff. %
H-75	E-11	1x2	1.80	42.1	23.4	6.20
H-76	E-11	.9x1.9	1.44	40.8	28.4	7.52
H-77	E-11	1x1	.90	22.6	25.1	6.68
H-78	E-11	1x1	.90	22.3	24.8	6.23
H-79	E-11	1x2	1.80	46.2	25.6	7.85
H-80	E-11	1x1	.90	23.3	25.9	7.70
H-81	E-11	1x1	.90	21.8	24.2	6.94
H-82	E-11	1x1	.90	22.5	25.0	7.46
*H-83	E-11	1x2	1.80	67.3	37.4	10.70
*H-84	E-11	1x2	1.80	67.2	37.4	10.80

*Cells fabricated without base region drift field.

In an effort to further reduce the amount of slice bowing which results from the strains induced in the substrate by the thick, highly doped epitaxial layer, smaller area substrate slices were utilized to fabricate the 10th lot of cells. This decreased the number of usable slices which could be obtained from each growth and did not seem to reduce the amount of bowing significantly. To minimize the effect of the bowing, the solar cell blanks were cut from the slices directly after the epitaxial growth and processed individually from that point on so that the inconsistancy in the distance between the active cell face and the epitaxial-substrate interface (which results from the plane parallel lapping) could be averaged. In the previous months the entire slice was reduced to the final thickness and the slices were cut into blanks subsequent to the reduction (see Step 8, First Phase Report). This latter method is much less time consuming but results in less control of the spacing, thus increasing the probability of obtaining cells in which the drift field is too far away from the p-n junction or else the substrate layer is lapped or etched entirely off in certain portions of the cell.

Current voltage curves of all sample cells submitted as lot 10 were obtained in both tungsten and solar simulator light systems. The results are summarized in Tables XVIII and XIX respectively. The efficiency degradations of the drift field cells in going from tungsten to m=0 solar simulator are between 8% and 16% which agree well with previous results.

Spectral response measurements made on the sample cells showed that the drift field cell responses peak in the 0.75 to 0.80 micron wavelength region and the field free control cells peak in the 0.84 to 0.85 wavelength region which is also in good agreement with measurements made on cells shipped priviously.

TABLE XVIII

STANDARD TUNGSTEN LIGHT SOURCE

100 mW/cm^2

Cell No.	Ingot No.	Dim. (cm)	Active Area (cm^2)	I_{sc} (mA)	I_{sc}/cm^2 (mA/cm^2)	V_{oc} (Volts)	I_{Pmax} (mA)	V_{Pmax} (Volts)	P_{max} (mW)	Eff. (%)
H-93	E-11	1x2	1.80	40.0	22.2	.523	36.0	.425	15.30	8.30
H-94	E-11	1x2	1.80	35.0	19.5	.500	31.6	.404	12.80	7.10
H-85	E-11	1x1.8	1.62	36.9	22.7	.498	31.5	.409	12.90	8.00
H-86	E-11	1x2	1.80	34.9	19.4	.506	29.1	.398	11.60	6.50
H-87	E-11	1x2	1.80	38.5	21.4	.507	33.4	.407	14.30	7.90
H-88	E-11	1x2	1.80	38.7	21.5	.523	32.5	.438	13.70	7.60
H-89	E-11	1x2	1.80	34.4	19.1	.521	30.4	.425	12.90	7.10
H-90	E-11	1x1.6	1.44	25.8	17.9	.492	22.5	.399	99.00	6.25
*H-91	E-11	1x2	1.80	59.0	32.8	.540	53.5	.445	23.80	13.20
*H-92	E-11	1x2	1.80	60.1	33.2	.540	56.0	.430	24.10	13.4

*Cell fabricated without base region drift field.

TABLE XIX

SOLAR SIMULATOR

140 mW/cm^2

Cell No.	I_{sc} (mA)	I_{sc}/cm^2 (mA/cm^2)	Eff. (%)
H- 93	48.2	26.80	7.50
H- 94	42.5	23.60	6.25
H-85	45.4	28.00	7.10
H-86	44.2	24.60	6.00
H-87	46.9	26.05	6.70
H-88	46.8	26.00	7.00
H-89	44.8	24.90	6.50
H-90	34.5	24.00	5.75
*H-91	66.3	36.80	10.50
*H-92	67.0	37.10	10.70

*Cells fabricated without base region drift field.

Upon examination of the dark reverse currents of the drift field cells of lot 10, it was found that all but one of these cells (Cell H-93) had unusually high reverse currents, indicating that leakage paths exist in the cells. From past experience with solar cells it has been found that such leakage paths normally occur across the edges of the cells and can usually be removed by grinding and re-etching the cell edges. In the case of these drift field cells, however, this was not found to be the case. The cells underwent a series of grinding and etching operations performed on the cell edges with dark reverse current measurements being made after each such operation. No significant improvement in the dark reverse current was observed. This leads to the conclusion that it is quite likely that the leakage paths exist in the body of the cell rather than at the edges. Such paths could be caused by strains induced by the lapping operation which are superimposed on strains which already exist due to the lattice mismatch between the lightly doped substrate region and the heavily doped epitaxial region. It would thus be advantageous to remove the last 2 or 3 mils of substrate thickness entirely by etching rather than lapping. However, since the contacting technique used required a fairly rough surface in order to provide good adherence, a final lap was necessary. Since this is likely the cause of the leakage paths, the investigation of polished etched surfaces was clearly indicated.

As mentioned previously, it was felt that it may be advantageous, from the point of view of minimizing the effects of strain at the epitaxi-substrate interfaces on the active part of the drift field cell, to remove the last few mils of excess substrate material by an etching technique rather than by lapping. However, since an etched surface provides poor adherence for the electrolessly plated contacts, a different technique for making electrical contact to the cell was required.

An evaporated-sintered silver-titanium contact is ideal electrically and mechanically for such a surface and this technique is used as a standard process in commercial solar cells. Therefore use was made of the process on drift field structures. However, because the surfaces are slightly different and the preliminary steps are substantially different it was found that this standard process did not work as well as norma After several attempts to use this technique on drift field cells and after several modifications, a workable contacting technique was arrived at which was then used in the fabrication of 5 of the 16 sample cells submitted as Lot 11. As a basis of comparison, the remaining 8 drift field cells were fabricated by utilizing the standard lapped surface in conjunction with the plated contact.

Current voltage curves of all sample cells submitted as Lot 11 were obtained in both tungsten and solar simulator light systems. The results are summarized in Tables XX and XXI respectively. The cells which were fabricated by utilizing the polish-etched surface and the evaporated-sintered contacting techniques are denoted in the tables. It can be seen that the open circuit voltages of the evaporated-sintered cells are considerably higher than those of the electrolessly plated cells indicating that the expectations proposed in monthly report No. 16 are true. In fact, cell H-102 actually has a considerably higher (by 20-25 mV) open circuit voltage than the field-free control cells and has an M = 0 efficiency of 9.8% which is extremely good. It would be very interesting and useful to determine the radiation damage characteristics of this cell. The average values of open circuit voltage, short circuit current density and maximum efficiency for the evaporated-sintered and electrolessly plated cells are 0.551 volts as opposed to 0.493 volts, 21.5 mA/cm^2 versus 21 mA/cm^2, and 8.1% against 7% respectively. Thus it can be seen that although there is little difference in current density between the two cell types, a significant difference exists in open circuit voltage and hence in efficiency. It would be interesting to carry out additional experiments along these lines to ascertain the reproducibility of the results and to definitely tie down the cause of these differences.

Spectral response measurements made on the sample cells showed that the drift field cell responses peak in the 0.75 to 0.80 micron wavelength region and the field-free control cells peak in the 0.84 to 0.85 wavelength region which is in good agreement with measurements made on cells shipped previously.

TABLE XX

STANDARD TUNGSTEN LIGHT SOURCE
100 mW/cm^2

Cell No.	Ingot No.	Dim. (cm)	Active Area (cm^2)	I_{sc} (mA)	I_{sc}/cm^2 (mA/cm^2)	V_{oc} (Volts)	I_{Pmax} (mA)	V_{Pmax} (Volts)	P_{max} (mW)	Eff. (%)
H-95	E-11	1x1	0.9	20.0	22.2	.480	16.4	.364	5.95	6.6
H-96	E-11	1x2	1.8	42.0	23.3	.480	37.2	.371	13.8	7.65
†H-97	E-11	1x2	1.8	43.0	23.9	.555	35.9	.441	15.88	8.8
†H-98	E-11	1x2	1.8	37.5	20.8	.550	31.5	.446	14.04	7.8
†H-99	E-11	1x1.8	1.62	32.5	20.1	.550	27.8	.422	11.73	7.2
H-100	E-11	1x1	0.9	21.5	23.9	.510	19.1	.409	7.81	8.65
†H-101	E-11	1x1.6	1.44	26.0	18.1	.530	22.5	.400	9.0	6.3
†H-102	E-11	1x2	1.8	44.5	24.7	.575	40.6	.470	19.04	10.6
H-103	E-11	1x1.7	1.53	27.5	17.9	.465	22.5	.354	7.96	5.2
H-104	E-11	1x2	1.8	33.0	18.3	.490	23.9	.368	8.8	4.9
H-105	E-11	1x2	1.8	36.5	20.2	.545	30.2	.437	13.2	7.3
H-106	E-11	1x2	1.8	40.0	22.2	.495	33.6	.384	12.9	7.2
H-107	E-11	1x2	1.8	36.0	20.0	.480	30.0	.370	11.1	6.2
*H-108	E-11	1x2	1.8	60.0	33.3	.555	55.1	.440	24.24	13.5
*H-109	E-11	1x2	1.8	59.0	32.8	.550	54.0	.445	24.11	13.4
*H-110	E-11	1x2	1.8	57.5	31.9	.550	54.0	.445	24.11	13.4

*Cell fabricated without base region drift field

†Cell fabricated with evaporated-sintered contacts

TABLE XXI

SOLAR SIMULATOR
140 mW/cm^2

Cell No.	I_{sc} (mA)	I_{sc}/cm^2 (mA/cm^2)	Eff. (%)
H-95	25.0	27.8	5.7
H-96	51.0	28.3	6.7
†H-97	54.5	30.3	8.3
†H-98	51.5	28.6	7.8
†H-99	43.7	27.0	7.3
H-100	27.0	30.0	8.0
†H-101	34.5	24.0	6.0
†H-102	56.5	31.4	9.8
H-103	37.5	24.5	5.5
H-104	43.5	24.2	5.1
H-105	48.3	26.8	7.3
H-106	52.0	28.9	6.9
H-107	45.5	25.3	5.7
*H-108	68.0	37.8	10.5
*H-109	67.0	37.2	10.4
*H-110	66.0	36.7	10.4

*Cell fabricated without base region drift field

†Cell fabricated with evaporated-sintered contacts

V. ANALYSIS OF DRIFT FIELD CELL CHARACTERISTICS

1.0 ANALYSIS OF THE A-FACTOR

The diode current-voltage relationship (excluding shunt and series resistance effects) is written as:

$$I = I_o\left[\exp(\frac{\beta V}{A})-1\right] \; ; \qquad \text{Eq. 5-1}$$

where β is a constant for a given temperature, I is the current at voltage V, I_o is the saturation current and A is the factor which represents the departure of the relationship from the theoretical ideal. In order to further analyze the electrical characteristics of the drift field cells, the magnitude of the A factor was determined in the following manner. The dark forward and reverse currents were obtained for drift field cell H-31. In Section IV it was noted that this cell had a poor curve shape which did not seem to be a result of either high series or low shunt resistance. It was therefore suspected that the poor curve shape might be due to a high A-factor value and would therefore provide a "worse-case" A-factor value.

Equation 5-1 can be written in the form:

$$V = \frac{A}{\beta}(\ell nI - \ell nI_o) \; ; \qquad \text{Eq. 5-2}$$

so that from a semi-log plot of the voltage-current relationship it is possible to obtain a measure of A since β has a room temperature value of about 40 $Volt^{-1}$. Also, at the V=0 intercept $I=I_o$, so that the reverse saturation current is also obtainable. It was found that for cell H-31 the appropriate A-factor was about 1.9 which was comparable to normal cell values. The saturation current density had a magnitude of 10^{-6} Amps. The saturation current is dependent, to a large extent on mobility, impurity concentration, and minority carrier lifetime. Normally it is

found that the latter parameter is most strongly affected by the cell processing technique since the dislocations and/or imperfections discussed above would also give rise to a reduction of minority carrier lifetime. Therefore, it was concluded that the poor curve shape might be due to the fabrication process itself, especially since the substrate material gave rise to high efficiency non-drift field cells. Considering the influence of ionized impurities, only, the I_o of the drift field cells should theoretically be lower than those of the control cells since the average number of ionized impurity atoms is expected to be greater for the former cell type.

2.0 ANALYSIS OF SPECTRAL CHARACTERISTICS

Since the spectral distribution of sunlight in space (Air Mass Zero) is considerably different, both on a relative and absolute basis, from either the spectral distribution of sunlight at the earth's surface (Air Mass One) or the spectral distribution of tungsten light at a filament color temperature of 2800°K, certain corrections must be applied to electrical measurements obtained under the latter two light systems in order to convert these to correspond to the values which would be obtained at Air Mass Zero outer space conditions.

In general the short circuit current of a silicon solar cell be expressed by the following equation:

$$I_{sc} = \int_0^\infty A(\lambda)R(\lambda)d\lambda \qquad \text{Eq. 5-3}$$

where $A(\lambda)$ is the spectral distribution of the light source and $R(\lambda)$ is the spectral response of the cell, both of these being in absolute units as a function of wavelength. Then the ratio of the short circuit current

of a solar cell obtained in two light systems can be obtained from Eq. 5-3 as:

$$\frac{I_{sc_1}}{I_{sc_2}} = \frac{\int_o^\infty A_1(\lambda)R(\lambda)d\lambda}{\int_o^\infty A_2(\lambda)R(\lambda)d\lambda} \quad ; \qquad \text{Eq. 5-4}$$

or replacing $R(\lambda)$ by $CR'(\lambda)$, where $R'(\lambda)$ is the spectral response in relative absolute units and C is a constant, as:

$$\frac{I_{sc_1}}{I_{sc_2}} \equiv K \equiv \frac{\int_o^\infty A_1(\lambda)R'(\lambda)d\lambda}{\int_o^\infty A_2(\lambda)R'(\lambda)d\lambda} \quad ; \qquad \text{Eq. 5-5}$$

where $A_1(\lambda)$ and $A_2(\lambda)$ represent the spectral distribution of light systems 1 and 2 respectively. It therefore is apparent that K is a correction factor which can be applied to the short circuit current obtained in System 2, to calculate the short circuit current which would be obtained in System 1. This correction factor has been determined for normal commercial solar cells with m=0 and m=1 sunlight as Systems 1 and 2 respectively, and has been found to be of the order of 1.19 to 1.21. If we assume that the efficiency is directly related to the short circuit current (a valid assumption for light levels normally encountered), this implies a decrease in efficiency of about 13 to 15% since the solar intensity at m=0 is 140 mW/cm^2 as opposed to 100 mW/cm^2 at m=1 (and hence if the efficiency in m=0 sun were identical to that in m=1 sun, K would have a value of 1.4). There is an additional observed degradation of about 6% in going from tungsten light (at 2800°K color temperature) to m=1 sunlight for a typical commercial solar cell so that the total decrease in cell efficiency in going from tungsten to m=0 sunlight is of the order of 19 to 21% giving rise to a K' value of 1.11 to 1.13 in going

from 100 mW/cm^2 tungsten light to 140 mW/cm^2 m=0 sunlight. These apparent degradations are, of course, a direct result of Eq. 5-1 and can be considered as the superposition of two phenomena, namely: (1) the spectral distribution of tungsten, m=1, and m=0 light becomes progressively greater in the shorter wavelength region and (2) the short to long wavelength cell response ratio is such as to give rise to a progressive decrease in cell I_{sc} per unit light intensity as the short to long wavelength ratio of the light source is increased.

In the case of the drift field cell, however, the spectral response is considerably different from the non-drift field cells, as can be seen from Figure 29, the former cell type having a higher short to long wavelength ratio due to poorer long wavelength collection efficiency. If we consider two non-drift field cells H-29 and H-30, it can be seen from Table IV and Table V (in the preceding section) which show the electrical characteristics of ten sample cells in both tungsten light and in an m=0 solar simulator, that the efficiency has undergone a decrease of about 19% and 24% respectively. If we consider the drift field cells, however, we find from Tables IV and V that the efficiency decrease is only 7 to 15% in going from tungsten to m=0 sunlight.

This range of efficiency decrease seems to hold true for almost all the drift field cells and verifies the spectral consistency of the drift field cells which was indicated by the spectral responses of these cells.

The drift field cells all exhibit peak responses between 0.75 and 0.80 microns and are lower in long wavelength response than the field-free control cells.

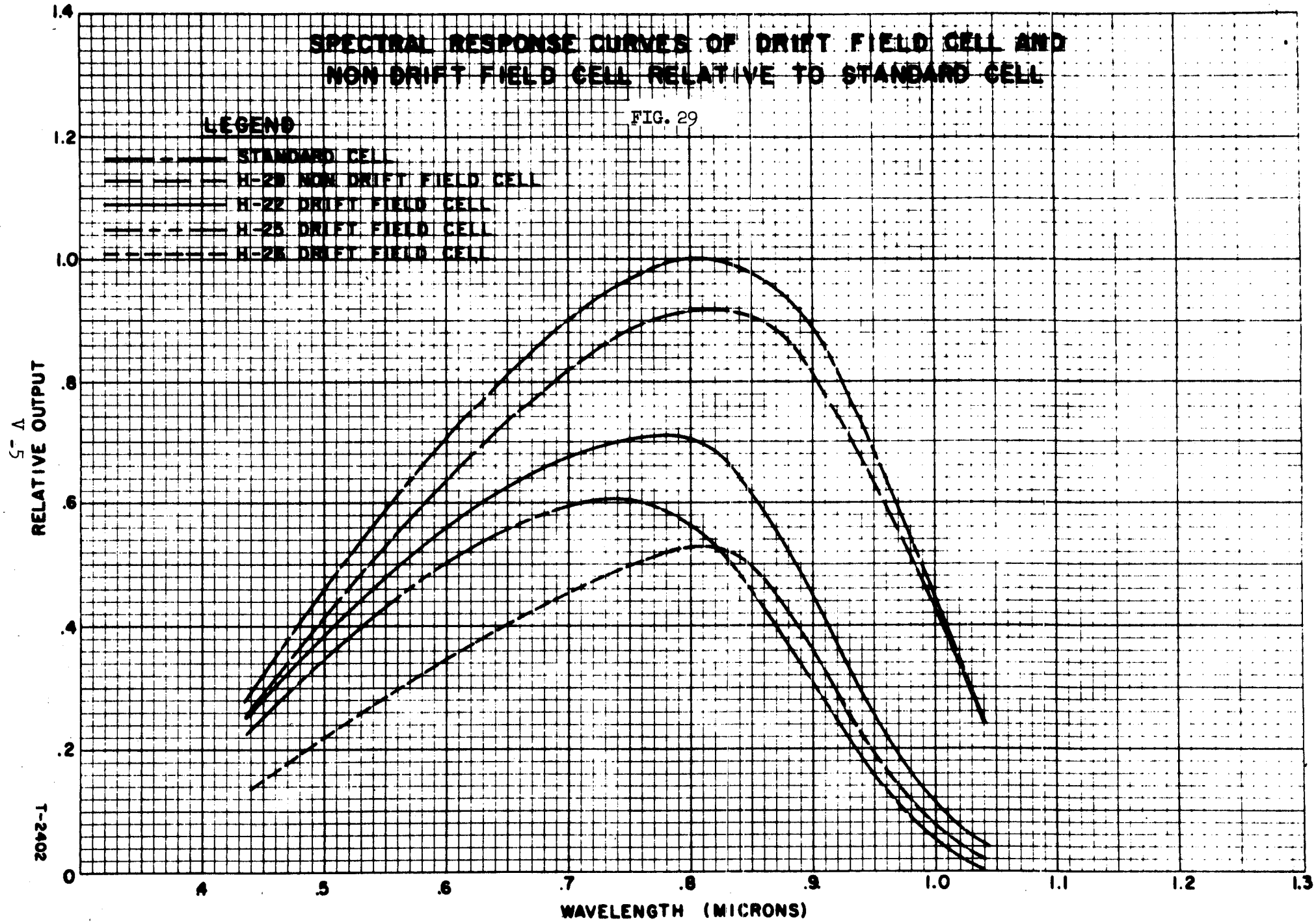
SPECTRAL RESPONSE CURVES OF DRIFT FIELD CELL AND NON DRIFT FIELD CELL RELATIVE TO STANDARD CELL
FIG. 29
LEGEND
STANDARD CELL
H-28 NON DRIFT FIELD CELL
H-22 DRIFT FIELD CELL
H-25 DRIFT FIELD CELL
H-26 DRIFT FIELD CELL
RELATIVE OUTPUT
WAVELENGTH (MICRONS)
1.4
1.2
1.0
.8
.6
.4
.2
0
.4
.5
.6
.7
.8
.9
1.0
1.1
1.2
1.3

T-2402

3.0 ANALYSIS OF EXPERIMENTALLY OBTAINED SHORT CIRCUIT CURRENTS

A theoretical determination has been made by Wolf[1] of the short circuit current density of various cell configurations under outer space conditions as a function of 1 MeV electron flux. These determinations are shown in Figure 30 The cases appropriate to the field-free cell and the drift field cell design adopted as the goal for this contract are curves A and D respectively. Since both these curves are perpendicular to the ordinate at 10^{12} e/cm^2, the respective current values at zero flux (pre-bombardment) condition should be identical to the current value at 10^{12} e/cm^2. The magnitude of the current densities before bombardment for the field free and drift field cells under m=0 sunlight should then be theoretically 42 and 34 mA/cm^2 respectively. Actually the theoretical value of 42 mA/cm^2 for the field-free cell is considerably higher than is actually experienced in practice. (An extraordinarily good cell will have a current density of 38.5 mA/cm^2 with a current density of 36 mA/cm^2 being more typical.) Because of the optimism of the theoretical values, it would be more meaningful to discuss the ratio of the short circuit currents rather than the absolute values for a study such as this. Considering the ratio of the currents theoretically expected for the drift field and field-free cells under m=0 sunlight, one obtains a ratio of 34/42 or 0.81. For comparitive purposes this ratio was determined on the drift field sample cells H-11 through H-61 by experimentally taking the ratio of the short circuit current densities as measured in the m=0 solar simulator to the current density expected in a field-free cell (36.0 mA/cm^2 typically and 38.5 mA/cm^2 for best case). These current density values represent typical and extraordinarily high values respectively of field-free experimentally observed m=0 short circuit currents. These comparitive ratios are presented in a condensed form in Table XXII The first column shows the cell identification ("H") number. The second and third columns

1) M.Wolf "Drift Fields in Solar Energy Converter Cells". Proceedings of the IEEE Vol. 51, No. 5, May, 1963.

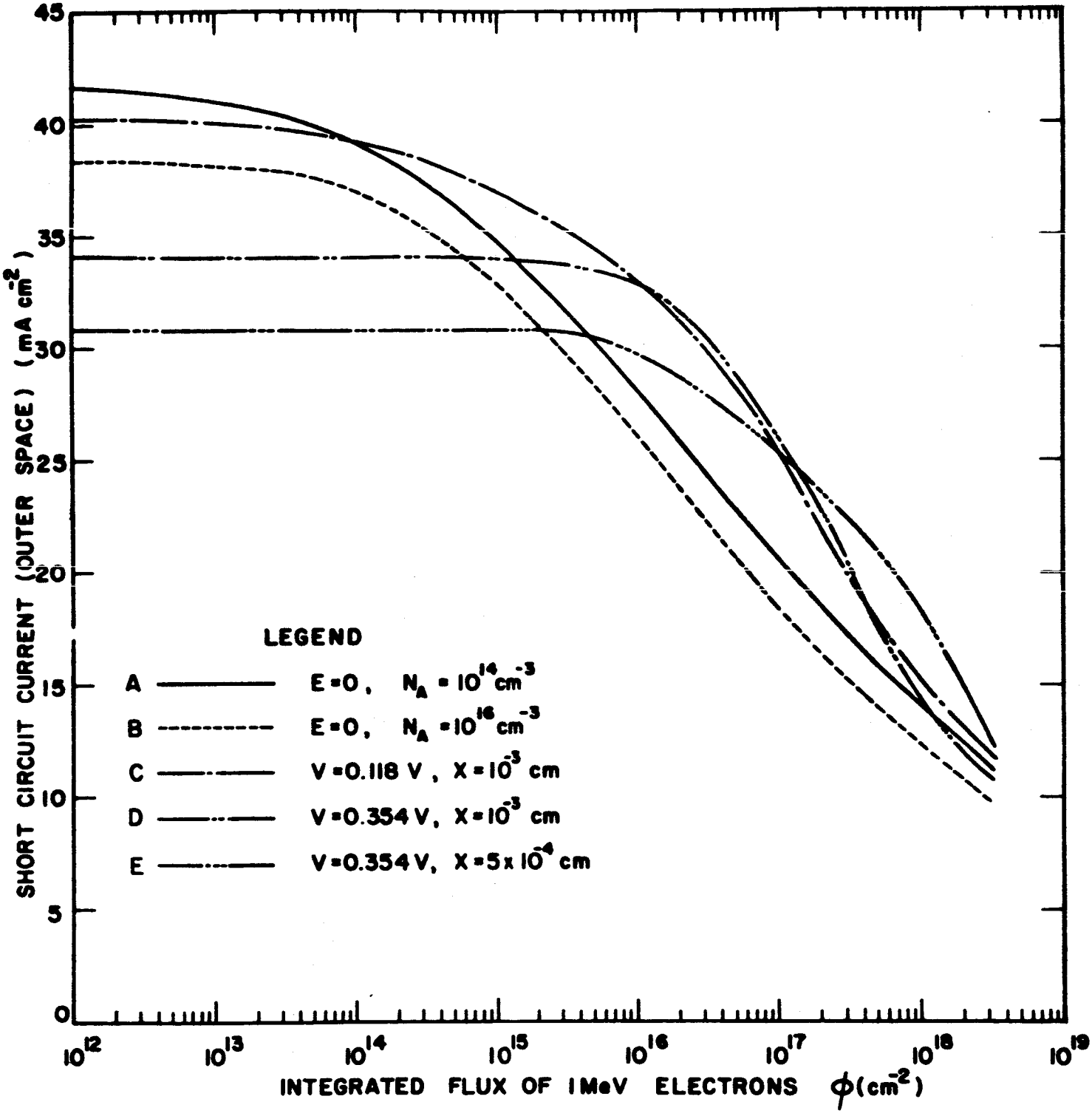
SHORT CIRCUIT CURRENT (OUTER SPACE) (mA cm^{-2})
45
40
35
30
25
20
15
10
5
0
LEGEND
A —— E=0, $N_A = 10^{14}$ cm^{-3}
B ---------- E=0, $N_A = 10^{16}$ cm^{-3}
C —·—·— V=0.118 V, X=10^{-3} cm
D —··—··— V=0.354 V, X=10^{-3} cm
E —···—···— V=0.354 V, X=5×10^{-4} cm
10^{12}
10^{13}
10^{14}
10^{15}
10^{16}
10^{17}
10^{18}
10^{19}
INTEGRATED FLUX OF 1MeV ELECTRONS ϕ(cm^{-2})

FIG. 30

T-2055

show the short circuit current densities and efficiencies respectively as measured in the m=0 simulator. The fourth and fifth columns indicate the ratio of the drift field short circuit current density to 36.0 and 38.5 mA/cm^2 current densities respectively. The fourth column represents the typical ratio while the fifth column represents the "worst-case" condition. Cells which have ratios which are greater than the theoretical 0.81 are denoted in the respective columns by an "x" immediately following the ratio value.

The fact that a good portion of the cells exhibit ratios which are in excess of the theoretically predicted currents shows that these cells have as good a short circuit current as can reasonably be expected on the basis of theory. It can be seen from the tables that the average ratio of all the drift field cells was 0.83 when the field-free cell current density of 36.0 mA/cm^2 was used and 0.77 when the field free cell current density of 38.5 was used. In the former case, 68% of the sample cells had a ratio equal to or greater than the theoretically expected value of 0.81 and in the latter case 47% of the sample cells had a ratio of 0.81 or greater. These figures lead to the encouraging conclusion that the experimentally observed reduction of the drift field short circuit currents below that of the field free control cells is in reality not much greater than one would expect theoretically and that an m=0 sunlight efficiency reduction of about 20% is not unreasonable in the case of the drift field cell, due simply to the short circuit current decrease.

4.0 ANALYSIS OF EXPERIMENTALLY OBTAINED OPEN CIRCUIT VOLTAGE

Table III-2 presents a summary of the open circuit voltages of all the drift field sample cells thus far submitted as well as the submitted control, field-free cells. A reasonable open circuit voltage for cells fabricated from 10 ohm-cm resistivity p-type silicon is of the order of 0.55 Volts. It can be seen from Table XVII that there is a considerable

TABLE XXII

DRIFT FIELD CELL SUMMARY SHEET

Theoretical Ratio $\frac{(I_{sc})_D}{(I_{sc})_{E=0}} = \frac{34}{42} = 0.81$ (m=0)

Typical $(I_{sc})_{m=0}$ of production cells 36 mA/cm^2 to 38.5 mA/cm^2

1	2	3	4	5
Cell Number	Experimental Cells (m=0) I_{sc}/cm^2	Efficiency (%)	Experimental Cells $(I_{sc})_D/(I_{sc})_{E=0}$ $(I_{sc})_{E=0}$ = 36.0	$(I_{sc})_{E=0}$ = 38.5
*H-61	31.7	8.2	.88 x	.82 x
*H-60	31.1	8.2	.87 x	.81 x
*H-59	29.4	7.9	.82 x	.77
H-58	32.8	8.4	.91 x	.85 x
H-57	31.9	8.1	.89 x	.83 x
*H-56	29.1	7.2	.81 x	.76
H-55	29.1	8.6	.81 x	.76
*H-54	28.7	5.9	.80	.74
H-51	42.5	11.7	1.18 x	1.10 x
*H-50	28.2	6.8	.78	.73
*H-49	29.7	7.1	.82 x	.77
H-48	32.4	8.6	.90 x	.84 x
H-47	30.9	6.5	.86 x	.80
H-46	28.1	6.8	.78	.73
H-45	30.6	8.2	.85 x	.79
H-43	33.0	8.7	.92 x	.86.x
H-42	30.2	8.1	.84 x	.78
H-41	31.9	9.4	.89 x	.83 x
H-37	33.4	8.2	.93 x	.87 x
H-36	29.4	6.6	.82 x	.76
H-35	28.2	5.5	.78	.73
H-34	29.4	5.9	.82 x	.76

TABLE XXII

(Continued)

1	2	3	4	5
H-33	23.2	4.4	.64	.60
H-32	23.9	5.4	.66	.62
H-31	21.7	4.6	.60	.56
H-28	36.7	9.8	1.01 x	.95 x
H-27	31.5	8.9	.87 x	.82 x
H-26	31.0	8.6	.86 x	.81 x
H-25	34.7	7.5	.96 x	.90 x
H-24	33.8	5.6	.94 x	.88 x
H-23	34.6	8.5	.96 x	.90 x
H-22	32.7	7.1	.91 x	.85 x
H-21	33.0	9.7	.92 x	.86 x
H-20	31.8	8.5	.88 x	.83 x
H-17	27.6	7.3	.76	.72
H-16	31.4	9.0	.87 x	.82 x
H-15	27.8	6.9	.77	.72
H-14	30.7	8.8	.85 x	.80
H-13	33.3	8.9	.92 x	.86 x
H-12	33.2	8.9	.92 x	.86 x
*H-11	31.6	8.9	.88 x	.82 x
m=1 H- 6	18.0	-	.50	.37
H- 5	25.0	-	.69	.65
H- 4	27.6	-	.77	.72
H- 3	22.2	-	.62	.58
H- 2	27.5	-	.76	.72
*H- 1	27.5	-	.76	.72
Average		7.6	.83	.77
			68% > .81	47% > .81

* indicates 1x2 cm cells

TABLE XXIII

OPEN CIRCUIT VOLTAGE

OF SAMPLE CELLS SHIPPED THUS FAR

Cell Number	Ingot Number	V_{oc} (Volts)	Cell Number	Ingot Number	V_{oc} (Volts)	Cell Number	Ingot Number	V_{oc} (Volts)
x H-1	E-3	.480	H-26	E-6	.511	H-51	E-6	.528
x H-2	E-3	.510	H-27	E-6	.523	*H-52	E-6	.551
x H-3	E-3	.430	H-28	E-6	.523	*H-53	E-6	.551
x H-4	E-4	.540	*H-29	E-6	.552	H-54	E-6	.516
H-5	E-4	.510	*H-30	E-6	.547	H-55	E-10	.538
H-6	E-4	.475	H-31	E-6	.470	H-56	E-10	.504
* H-7	E-3	.387	H-32	E-6	.490	H-57	E-10	.502
* H-8	E-3	.370	H-33	E-6	.430	H-58	E-10	.498
* H-9	E-4	.537	H-34	E-6	.440	H-59	E-10	.531
*H-10	E-4	.545	H-35	E-6	.440	H-60	E-10	.508
H-11	E-5	.522	H-36	E-6	.500	H-61	E-10	.501
H-12	E-5	.520	H-37	E-6	.510	*H-62	E-10	.538
H-13	E-5	.510	H-38	E-6	.500	*H-63	E-10	.540
H-14	E-5	.523	*H-39	E-6	.540	*H-64	E-10	.540
H-15	E-5	.450	*H-40	E-6	.545	xH-65	E-10	.561
H-16	E-5	.516	xH-41	E-7	.555	H-66	E-10	.530
H-17	E-5	.482	H-42	E-7	.542	xH-67	E-10	.552
*H-18	E-5	.559	H-43	E-7	.537	xH-68	E-10	.548
*H-19	E-5	.558	*H-44	E-7	.550	H-69	E-10	.531
H-20	E-5	.480	xH-45	E-6	.560	H-70	E-10	.542
H-21	E-6	.530	H-46	E-6	.518	H-71	E-10	.547
H-22	E-6	.480	H-47	E-6	.535	H-72	E-10	.540
H-23	E-6	.520	H-48	E-6	.535	*H-73	E-10	.544
H-24	E-6	.460	H-49	E-6	.535	*H-74	E-10	.547
H-25	E-6	.485	H-50	E-6	.533			

* indicates control cells.

x indicates V_{oc} greater than control cells.

spread in the open circuit voltages of the drift field cells but that the average value of open circuit voltage is only of the order of .505 Volts or about 10% less than observed for field-free cells. A rigorous theoretical treatment of the open circuit voltage which one should expect of a drift field cell of a given design has not yet been carried out. The problem is somewhat different from the case of the short circuit current theory since the effect of the Fermi level variation as a function of distance from the junction on the resultant open circuit voltage has not yet been described mathematically. The current voltage characteristic of a solar cell exclusive of series and shunt resistance terms is given by Wolf and Prince [5] as:

$$I = I_o(e^{qV/AkT}-1)-I_L \quad ; \qquad \text{Eq. 5-6}$$

where I is the cell current at voltage V, q is the electronic charge, A is a constant which describes the departure of the junction from ideality, k is Boltzmann's Constant, T is the temperature in degrees Kelvin, I_o is the reverse saturation current and I_L is the light generated current. Under open circuit conditions the external current flow, I, is zero by definition and the equation may be written:

$$V_{oc} = \frac{AkT}{q} ln(\frac{I_L}{I_o}+1) \quad ; \qquad \text{Eq. 5-7}$$

since

$$\frac{I_L}{I_o} >> 1 \qquad \text{Eq. 5-8}$$

the equation can be written:

$$V_{oc} = \frac{AkT}{q} \quad \frac{I_L}{I_o} \qquad \text{Eq. 5-9}$$

---

5) M. Wolf and M. B. Prince, "New Developments in Silicon Photovoltaic Devices and Their Application in Electronics" , J. Brit. IRE, Vol. 18 October, 1958.

Since at a given temperature I_o is given by:

$$I_o = K\left(\sqrt{\frac{\mu_p}{\tau_p}} \cdot \frac{1}{N_n} + \sqrt{\frac{\mu_n}{\tau_n}} \cdot \frac{1}{P_p}\right) \quad ; \qquad \text{Eq. -10}$$

where K is a constant, μ_p and μ_n are the hole and electron minority carrier mobilities respectively, N_n and P_p are the majority carrier densities of ionized donor and acceptor atoms respectively and τ_p and τ_n are the hole and electron minority carrier lifetimes respectively. Then for a specific temperature, Eq. 5-9 can be written:

$$V_{oc} = \frac{AkT}{q} \ln \frac{I_L}{K\sqrt{\frac{\mu_p}{\tau_p}} \cdot \frac{1}{N_n} + \sqrt{\frac{\mu_n}{\tau_n}} \cdot \frac{1}{P_p}} \qquad \text{Eq. 5 -11}$$

Thus it can be seen that the open circuit voltage increases with increasing light generated current, minority carrier lifetime, and density of ionized majority carriers (which is inversely proportional to the material resistivities of the respective regions) while it decreases with increasing minority carrier mobility.

For a drift field cell having a design similar to the one developed for this contract the parameters will be different from those of a 10 ohm-cm base material field-free cell. In the case of the drift field cell, theory predicts that the I_L will be about 20% lower as discussed in the previous section. The minority carrier lifetime will decrease due to the additional impurity atoms introduced in order to form the field, and possibly due to the strains introduced by the epitaxial deposition process. The minority carrier lifetime of control field-free cells made during this program has been measured by the Kingston method[6] and was found to be of the order of 16 μ-sec which is typical of good commercial

---

6) R. H. Kingston, "Switching Time in Junction Diodes and Junction Transistors", Proceedings of the IRE, Vol. 42, No. 5, May 1954

N/P solar cells. Since this test method requires the destruction of the cell under test, a high efficiency drift field cell has not yet been measured but it is expected that the base region minority carrier lifetime of these cells would be reduced by a factor of about 1/10 over that of the control cells. These differences will tend to decrease the V_{oc} of the drift field cells over that of the field-free controls according to Eq. 5-11. The mobility would also be expected to be different for the drift field cell case and it would be expected to decrease, due to the increased concentration of the impurity atoms which form the field. This effect, however, should only be of a second or third order. The number of ionized impurity atoms will, needless to say, increase. The mobility and number of ionized impurity atoms are thus expected to change in such a way as to increase the V_{oc} of the drift field cell. The value of the parameters μ_n, τ_n and P_p will vary across the field and thus can only be analytically described as a function of the distance along the axis normal to the plane of the N/P junction.

It is known from previous experiments that the addition of impurities to the base region of a cell at a distance of about 300μ away from the junction has no effect on the open circuit voltage of a cell. It is also known experimentally that the uniform addition of impurities to the entire base region of a cell will result in an increase of open circuit voltage. It can therefore be safely assumed that the effect of the addition of impurity atoms on the open circuit voltage is dependent upon the distance between these atoms and the junction. While a functional relationship between junction-impurity distance and V_{oc} is not known at the present time, it is possible to determine the limits of the effect of addition of impurities on the open circuit voltage.

If we consider some sort of averaging process, the apparent density of ionized impurity atoms would be increased in the base region substrate by about a factor of 10^2 atoms per cubic centimeter. This assumption

that the density of ionized impurity atoms is averaged throughout the substrate base region will give a maximum value for the open circuit voltage and will correspond to the upper limit.

If we consider only the changes experienced in the P region of the cell, Eq. 5-11 can be used to show the open circuit voltage change expected according to the following expression:

$$V_{oc}-V_{oc}' = \frac{AkT}{q}\left[\ln\frac{I_L}{K\sqrt{\frac{\mu_n}{\tau_n}}\cdot\frac{1}{P_p}} - \ln\frac{I_L'}{K\sqrt{\frac{\mu_n'}{\tau_n'}}\cdot\frac{1}{P_p'}}\right] \qquad \text{Eq. 5-12}$$

or

$$V_{oc}-V_{oc}' = \frac{AkT}{q}\ln\frac{\dfrac{I_L}{\sqrt{\frac{\mu_n}{\tau_n}}\ \frac{1}{P_p}}}{\dfrac{I_L'}{\sqrt{\frac{\mu_n'}{\tau_n'}}\ \frac{1}{P_p'}}} \qquad \text{Eq. 5-13}$$

where the primed quantities represent the parameters appropriate to the drift field cell and the unprimed quantities represent those appropriate to the field-free cell. Using the approximate values given above:

$$\tau' = \frac{\tau}{10} \qquad I_L' = .8I_L \qquad P' = Px10^2$$

and an A-factor of unity

$$\frac{AkT}{q} = \frac{1}{40} \quad \text{at room temperature}$$

$$V_{oc}-V_{oc}' = \frac{1}{40}\ln.04 = -.075 \text{ Volts} \qquad \text{Eq. 5-14}$$

In other words, the assumption that the density of impurities can be averaged leads to the conclusion that the open circuit voltage of the

drift field cells should be higher than that of a field-free cell by about .075 Volts. This represents an upper limit to the difference in open circuit voltage between drift field and field-free cells.

In the above analysis the term involving the number of ionized impurity atoms has the dominating effect on the V_{oc} change since it represents the largest order of magnitude change as well as entering into the natural logarithm term as a unity power rather than as square root term (as does the minority carrier lifetime term which is the only other term that can vary by an order of magnitude or more).

On the other hand, one can also consider the case where the distribution of the additional impurity atoms is such that there is no addition to the number of ionized impurity atoms in the base region. This would be the situation if the atoms were introduced too far away from the junction to be ionized, or in other words, well outside of the space charge region.

In this case P' = P with the other parameters having values similar to those previously used. Then Equation 3-13 yields:

$$V_{oc}-V_{oc}' = \frac{1}{40} \ln 4 = .035 \text{ Volts} \qquad \text{Eq. 5-15}$$

Here it can be seen that rather than obtaining an increase in open circuit voltage for the drift field cell over the field-free cell, as was calculated for the uniform impurity density assumption, in this instance a decrease in open circuit voltage of .035 Volts is predicted for the drift field cell.

Hence, depending upon the spatial distribution of the introduced impurity atoms with respect to the distance normal to the plane of the junction, the open circuit voltage of the drift field cell can be higher than that of the field-free cell by as much as .075 Volts and lower than the field-free cell by as much as.035 Volts.

As stated previously the open circuit voltages of the sample drift field cells have quite a large spread in values. This is not too surprising in view of the large range between the theoretical limits of the V_{oc} as discussed above. On rare occasions the V_{oc} of the drift field cells (made from 10 ohm-cm starting material) have been found to exceed the V_{oc} of the sample cells by about .01 Volts (drift field cells H-45 and H-65) thus showing that it is possible for drift field cells of this type to have a higher voltage than the field-free cells in actual practice. The drift field cells which have open circuit voltages greater than one of the control cells are denoted by an "x" preceding the cell number in Table XVII. It was shown in the first phase report that the open circuit voltages of drift field cells fabricated from approximately 200 ohm-cm material (Cells H-1, H-2, H-3) were consistently higher than those of control cells (H-7 and H-8) made from the same material.

Since the short circuit currents of the drift field cells seem to be approaching the theoretically expected values as discussed in the preceding section, it is quite possible that further increases in drift field cell efficiency will be a result of increased open circuit voltages.

5.0 PROCESS ANALYSIS

In processing the drift field cells it is necessary to separate, as much as possible, the effects of process variables from the effects due to the cell design itself. In order to achieve this end, the effects of the two most important variables, namely the starting material itself and the N/P junction diffusion, have been separated out by means of control cells. Field-free control cells were fabricated from each of the ingots which were utilized as drift field substrates. These control cells were utilized to evaluate the starting material and insure its applicability to the program, and further serve to provide field-free control cells for comparison of electrical performance and radiation characteristics. Control cells were also diffused at the same time as

the N/P junction diffusion of the drift field cells in order to insure that the diffusion was up to the standard required to produce high efficiency cells. Control cells were also utilized in the other processing steps such as contact deposition, junction clean-up, anti-reflectance coating and etc. These control cells have been of great value in analyzing the characteristics of the drift field cells, especially when the cells were somewhat lower in efficiency than normally encountered. While control cells do not always explain all contingencies, they can be used to provide information as to "what did not go wrong" and give a basis for comparitive analysis.

6.0 PRELIMINARY ANALYSIS OF CELL DESIGN ON ELECTRICAL PARAMETERS

A preliminary experiment was performed to determine the effect of the location of the drift field with respect to the electrical p-n junction on the various cell electrical parameters. Also investigated was the effect of thick and thin epitaxial layers on the electrical characteristics.

Four cells having an epitaxial layer of about 10 mils thickness and 4 cells having an epitaxial layer of about 7 mils thickness were fabricated. These cells had substrate thickness of about 1 to 1.5 mils. Five cells were also fabricated with substrate thicknesses of about 3 mils and epitaxial layer thicknesses of about 10 mils. The results are summarized in Table XXIV. There seems to be little significant difference between the cells made with 10 mil epitaxial layers and those made with 7 mil epitaxial layers. On the other hand the cells having 3 mil substrates show a significant trend towards higher efficiencies than those having 1 mil substrates. This is achieved through both higher short circuit currents and open circuit voltages. The fact that the cells having 3 mil substrates exhibit higher currents and efficiencies than the cells having 1 mil substrates was predicted by theory and is a result of the fact that the edge of the drift field in the former case is 2.5 mils away from the electrical junction and therefore gives rise to a larger average base region minority carrier lifetime (since in this case carriers created in the first 2.5 mils of base region pass only through

the relatively high purity substrate material and not through the highly doped drift field region). Also strains existing at the epitaxi-substrate interface are less likely to propagate crystalline imperfections throughout the active portion of the cells in the cells having the thicker substrates.

Since the cells for this experiment were fabricated from epitaxial slices which had shown a slight degree of bowing, there may have been some variation in the distance between the edge of the field and the electrical junction, so that the experimental results are only qualitative in nature.

TABLE XXIV

TUNGSTEN LIGHT

Cell No.	Approximate Thickness: Epitaxial Layer (mils)	Approximate Thickness: Substrate Layer (mils)	Cell Active Area (cm^2)	I_{sc} (mA)	V_{oc} (Volts)	$I_{P_{max}}$ (mA)	$V_{P_{max}}$ (Volts)	P_{max} (mW)	Eff. (%)
1	7	1	1.8	29.9	0.463	19.5	0.340	5.65	3.10
2	7	1	1.8	43.8	0.508	39.3	0.401	15.70	8.75
3	7	1	1.8	33.3	0.539	29.2	0.429	12.50	6.95
4	7	1	1.8	----	----- Broken in processing			-----	----
5	10	1	1.8	36.8	0.493	30.8	0.382	11.77	6.50
6	10	1	1.8	----	Extremely low current and voltage				----
7	10	1	1.8	34.0	0.440	<--- Broke during measurement			----
8	10	1	1.8	37.7	0.550	30.9	0.443	13.70	7.60
9	10	3	1.8	42.2	0.554	38.3	0.452	17.30	9.60
10	10	3	1.8	42.2	0.560	38.2	0.462	17.70	9.80
11	10	3	1.8	39.8	0.547	36.8	0.446	16.40	9.10
12	10	3	0.9	20.9	0.530	18.7	0.428	8.00	8.80
13	10	3	0.9	19.0	0.500	14.0	0.403	5.65	6.30

VI. ANALYSIS OF RADIATION CHARACTERISTICS

Radiation experiments have been performed by NASA Goddard on cells selected from sample lots one, three and four. The results are analyzed below.

Eight cells selected from Heliotek lot 1 (see monthly report No. 5) were bombarded with 1 MeV electrons in the first radiation experiment. Of these 8 cells, only 3 of these (H-4, H-5 and H-6) were representative of the near optimum design drift field cells which were fabricated throughout the remainder of the contract. Three cells (H-1, H-2 and H-3) were fabricated from very high resistivity (greater than 200 ohm-cm) material and hence had very low initial efficiencies due to extremely high series resistance values, and 2 cells (H-7 and H-9) were control cells containing no drift field region. Cells H-4 and H-5 were quite similar in efficiencies throughout the range of electron fluxes investigated, while H-6 was considerably lower in pre-bombardment efficiency and was therefore lower in efficiency throughout the experiment.

A comparison of the behavior of the best Heliotek cell (H-4 with the best cell from each of the other laboratories in this first radiation experiment, (Electro-Optical Systems, Radio Corporation of America, and Texas Instruments) is presented in the following figures. Fig. 31 presents the cell efficiency in a 100 mW/cm^2 xenon light source as a function of 1 MeV electron flux as obtained from the NASA measurements. The efficiency seems to vary somewhat linearly with the logarithm of the flux and a straight line approximating the behavior has been drawn in the semilog plot. It can be seen that the Heliotek drift field cell maintains a higher cell efficiency through the flux range considered.

Figure 32 shows the short circuit current density on an absolute basis as a function of the electron flux. In this case the Heliotek cell is lower than the RCA and EOS cells at a flux level of 5×10^{14} e/cm^2, but crosses over the EOS and RCA cell curves at fluxes of 10^{15} and 5×10^{15} e/cm^2 respectively. The slope of the line approximating the function is much

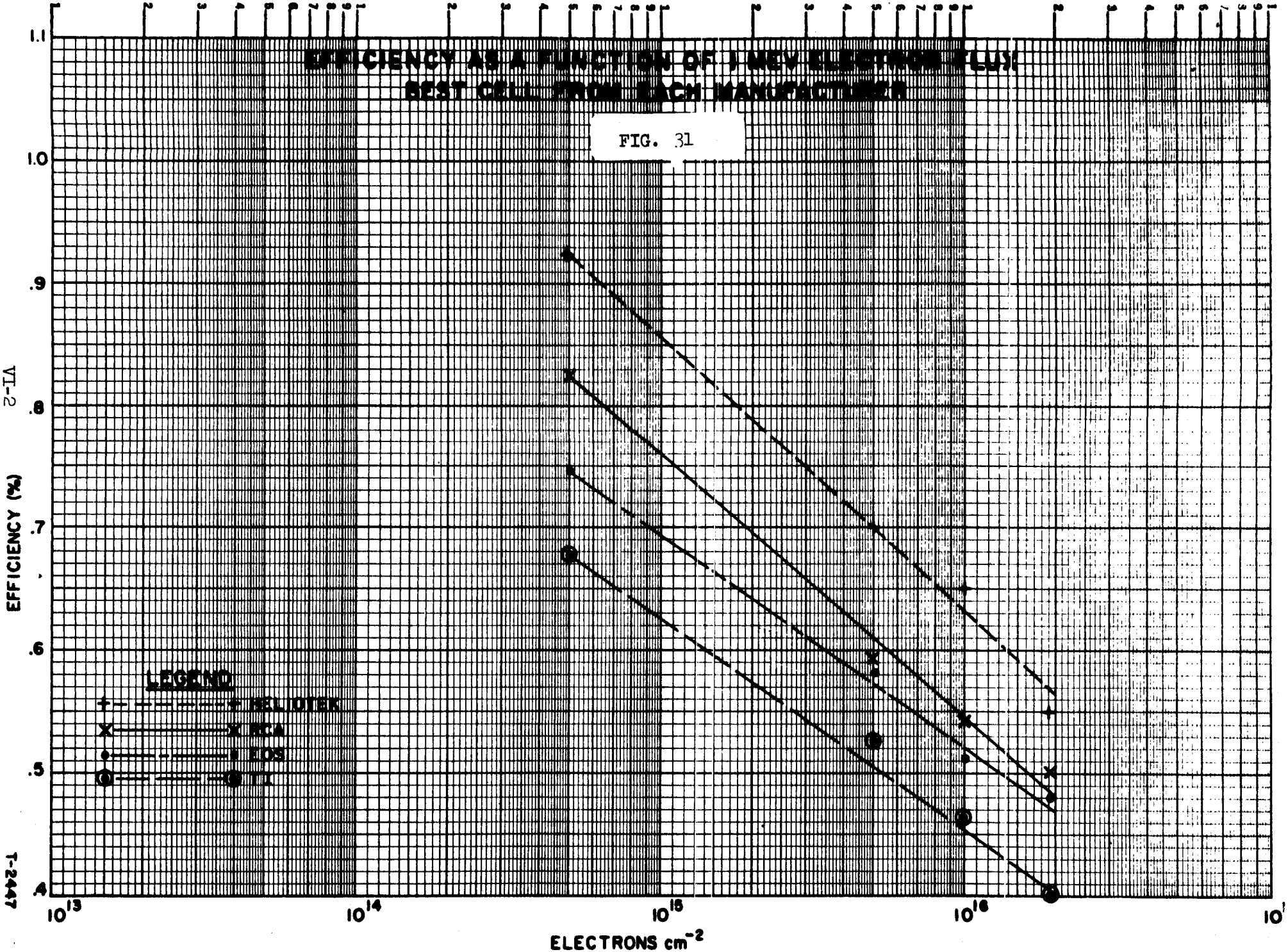

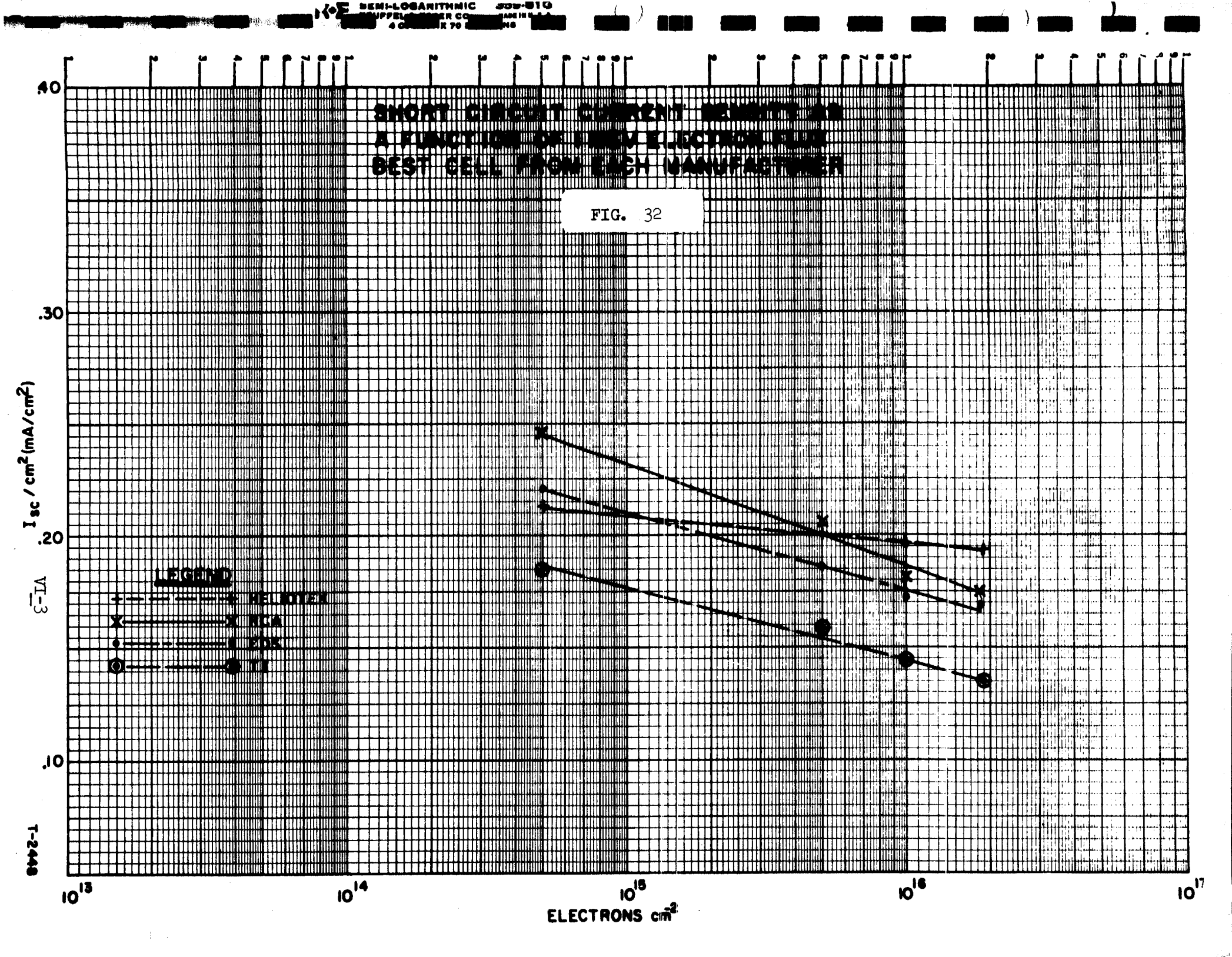

shallower in the case of the Heliotek cell than in the case of the other cells which have slopes which are quite similar to one another. This indicates that current collection, in the case of the Heliotek cell, is not as dependent upon the flux level for the range considered in this experiment, which was predicted theoretically previous to the start of the contract[1]. According to theory, a lower short circuit current was anticipated initially with no significant change in short circuit current expected with the Heliotek cell design until fluxes greater than 10^{16} e/cm^2 were encountered.

This would result in a crossover between the drift field cell curves and the standard type N^+/P cell curve at a flux level of about 5×10^{14} e/cm^2. The drift field cell curve was expected to stay above the standard cell curve at higher fluxes, but eventually at about a flux of 10^{18} e/cm^2 the two curves would again approach each other. See Figure 30 (preceding section) for cell design V=0.342V and X=10^{-3}cm compared to standard N^+/P cell design of E=0 and $N_A=10^{16}$ cm^{-3}. Therefore, over the range of fluxes investigated, it appears that the experimental results are close to that expected by theory.

The ratio of the short circuit current to the pre-bombardment short circuit current is shown as a function of electron flux in Fig. 33 Again the slope of the function is considerably shallower for the Heliotek cell than for the other three types of cells which have slopes quite similar to one another.

The conclusion that may be drawn from this preliminary data is that the short circuit current behavior of the Heliotek cell under 1 MeV electron irradiation was considerably different from that of the other cells for flux levels between 5×10^{14} and 1.88×10^{16} e/cm^2, and that the relative

---

1) Wolf, M., "drift Fields in Photovoltaic Solar Energy Converter Cells", Proceedings of the IEEE Vol. 51, No. 5, May, 1963

RATIO OF SHORT CIRCUIT CURRENT TO PRE-BOMBARDMENT SHORT CIRCUIT CURRENT AS A FUNCTION OF 1 MEV ELECTRON FLUX BEST CELL FROM EACH MANUFACTURER

FIG. 33

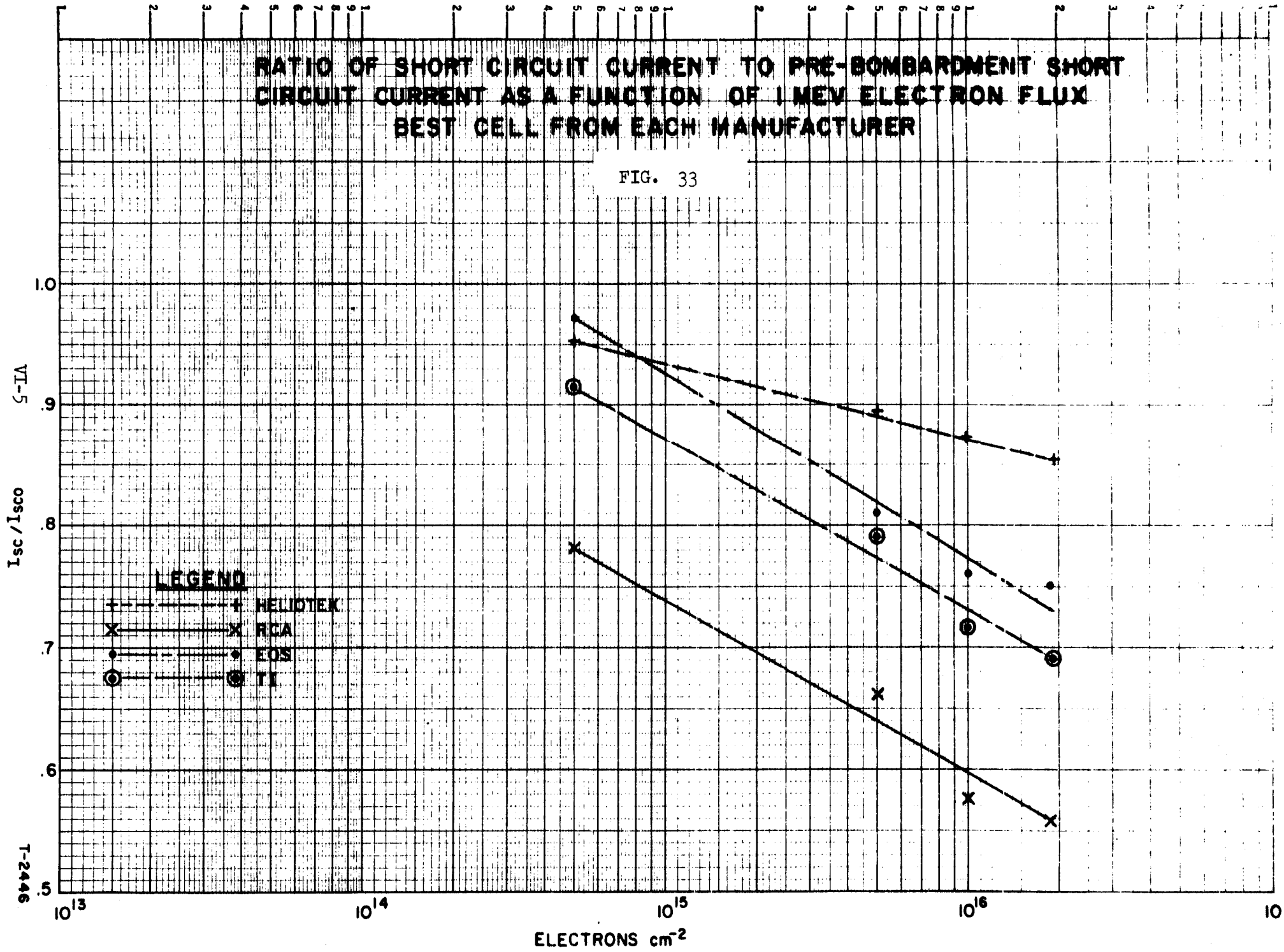

insensitivity of the Heliotek cell short circuit current to flux levels of the order of 10^{16} e/cm^2 was in close agreement with the theoretical predictions. It should be further noted that the other two applicable Heliotek sample cells (H-5 and H-6) exhibit slopes almost identical to that of cell H-4 and were merely shifted on the ordinate scale by a constant factor, thus showing the consistency of the radiation characteristics from cell to cell.

3.1 RESULTS OF SECOND RADIATION EXPERIMENT

Cells from the third and fourth lot of Heliotek sample cells were evaluated in the second radiation experiment which considered 1 MeV electron fluxes up to the order of 10^{16} e/cm^2. The data obtained indicates that the cells from these third and fourth groups not have the same radiation characteristics as did the cells from the first group and that the cells from the third lot were superior to those of the fourth lot.

Figure 34 shows the absolute short circuit current density as a function of electron flux as obtained from the NASA data. As in the analysis of the first radiation experiment, a linear relationship was assumed between the short circuit current density and the logarithm of the flux. The highest efficiency cells at an electron flux of about 10^{16} e/cm^2 from the sample cells submitted by Electro Optical Systems. Texas Instruments and Heliotek are also plotted in this graph. Also shown for basis of comparison are the curves appropriate to Heliotek field free control cells from the fourth lot and Heliotek drift field cell H-4 which exhibited the best radiation characteristics of all the cells considered in the first radiation experiment. In analyzing the NASA radiation data, it seemed rather clear from the current voltage and quantum yield curves that the data on Texas Instruments Cells Numbers 22 and 24 corresponding to

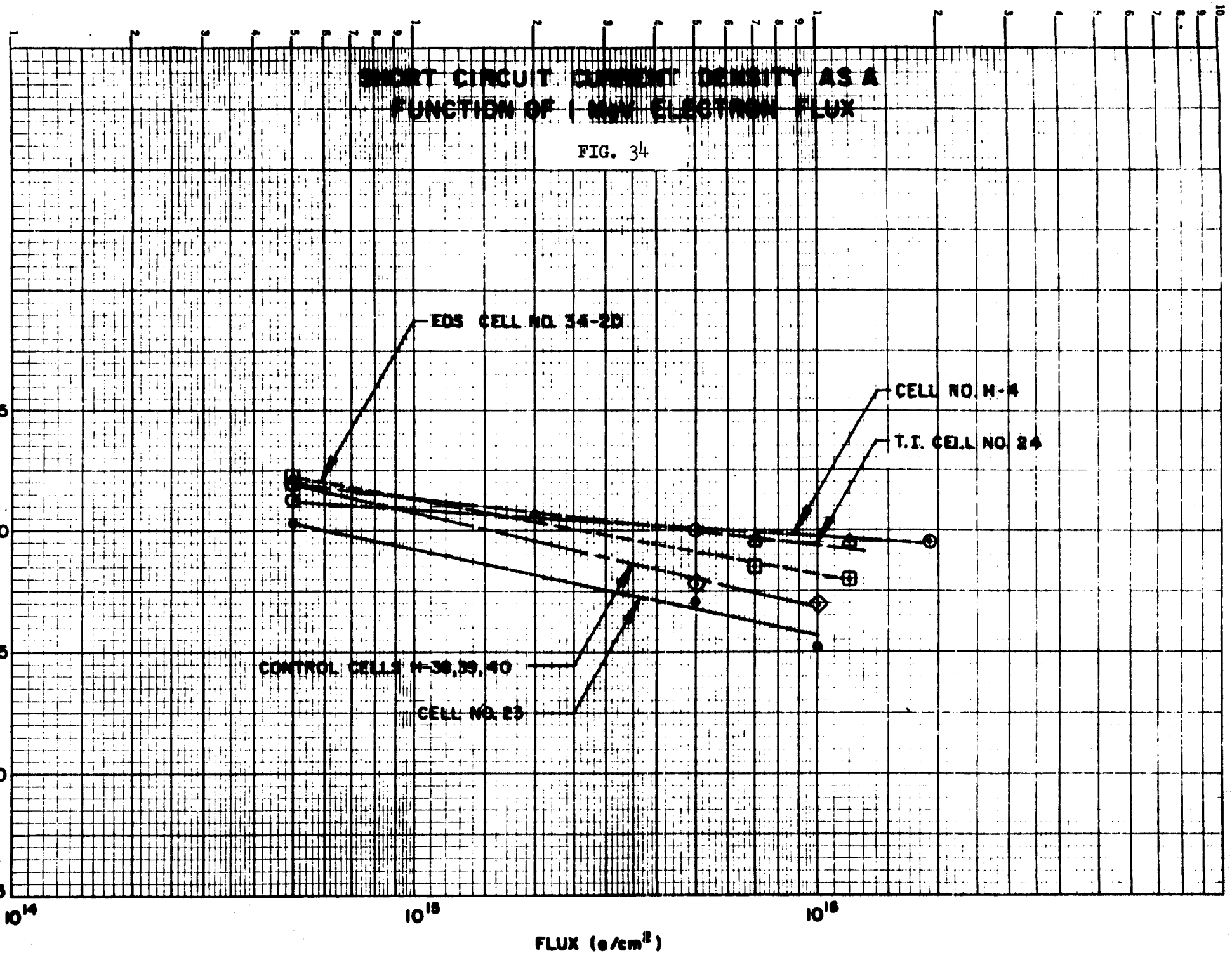
SHORT CIRCUIT CURRENT DENSITY AS A FUNCTION OF 1 MeV ELECTRON FLUX
EOS CELL NO. 34-2D
CELL NO. H-4
T.I. CELL NO. 24
CONTROL CELLS H-38,39,40
CELL NO. 23
SHORT CIRCUIT CURRENT DENSITY (mA/cm²)
FLUX (e/cm²)
5
10
15
20
25
10¹⁴
10¹⁵
10¹⁶

FIG. 34

the 1.2×10^{16} e/cm^2 bombardment flux had been interchanged, and hence the curves appropriate to TI cell No. 24 were plotted by assuming this to be the case. It can be seen from Figure 34 that Heliotek cell H-4 exhibited the least change in short circuit current density over the flux range considered. The TI cell exhibited a slightly steeper slope. The EOS cell exhibited a steeper slope than either of these but was not as steep as the Heliotek cell H-23 which was evaluated during this second series of bombardments. Cell H-23 did not have a slope too signigicantly different from the Heliotek field-free control cells H-38, H-39 and H-40. The marked difference between the behavior of cells H-4 and H-23 cannot really be analyzed and fully understood unless the cells themselves can be cross-sectioned in order to observe possible structural differences. It is possible that slice bowing resulting from strains occurring during the epitaxial process (see Reports 11 and 13) caused a variation in the thickness of the substrate, and hence caused a variation in the position of the drift field with respect to the junction, thus giving rise to the poorer short circuit current radiation characteristics of cell H-23.

An extremely interesting phenomenon is observed if one considers the open circuit voltages of these cells as a function of electron flux as shown in Figure 35. It is seen from this figure that cell H-4 which had the least sensitivity to the irradiation on a short circuit current basis shows the most sensitive behavior on an open circuit voltage basis. Similarly, the Texas Instruments cell No. 24 which showed the second best radiation characteristics with respect to current density showed the second worst behavior with respect to open circuit voltage, with the slope of the function being quite similar to that exhibited by cell H-4. The slope of the EOS cell and the field-free Heliotek control cells were almost identical and were considerably shallower than Texas Instruments cell 24 and Heliotek cell H-4. Heliotek cell H-23 exhibited a slightly steeper slope than the field-free control cells and the EOS cell but a significantly shallower slope than H-24 or Texas Instrument cell No. 24. In general,

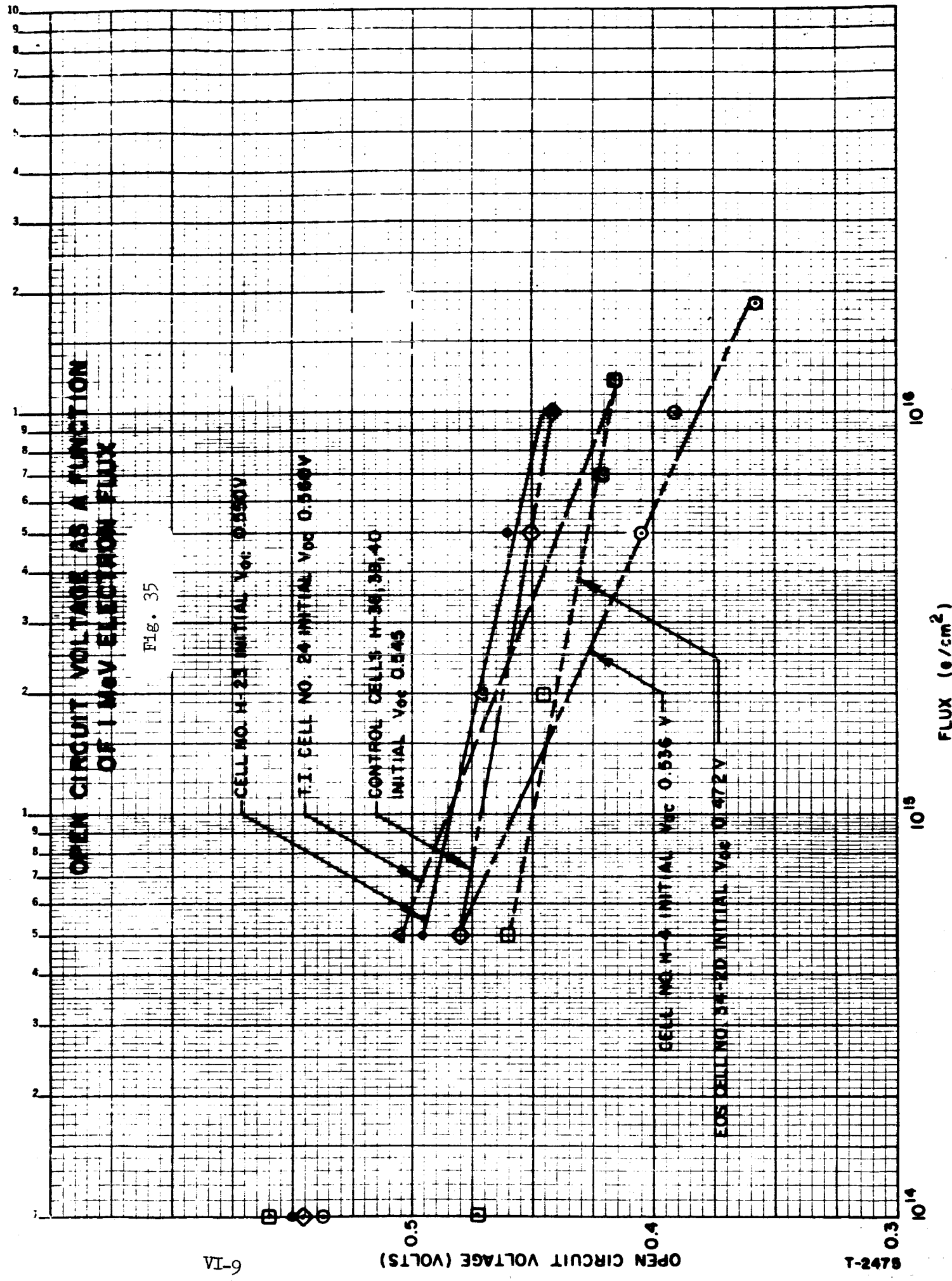
OPEN CIRCUIT VOLTAGE AS A FUNCTION OF 1 MeV ELECTRON FLUX
CELL NO. H-23 INITIAL Voc 0.550V
T.I. CELL NO. 24 INITIAL Voc 0.560V
CONTROL CELLS H-36, 38, 40 INITIAL Voc 0.545
CELL NO. H-4 INITIAL Voc 0.536 V
EOS CELL NO. 54-20 INITIAL Voc 0.472 V
OPEN CIRCUIT VOLTAGE (VOLTS)
FLUX (e/cm²)
0.5
0.4
0.3
10¹⁴
10¹⁵
10¹⁶
T-2475

Fig. 35

shallower slope than H-24 or Texas Instrument cell No. 24. In general, then, it seems that the cells which show the best radiation characteristics with respect to short circuit current density exhibit the poorest radiation behavior with respect to open circuit voltage. According to theory[1] the edge of the base region drift field should be in close proximity to the p-n junction in order to obtain the most advantageous current collection at 1 MeV flux levels of the order of 10^{16} e/cm^2. No prediction was made for the effect of the drift field width, strength, and placement on the open circuit voltage as a function of irradiation flux. It is quite likely, in view of the experimentally observed phenomena, that some of the parameter requirements which lead to an advantageous short circuit current versus flux relationship give rise to a disadvantageous open circuit voltage versus flux behavior. One such parameter might well be the distance between the edge of the base region drift field and the electrical p-n junction since this is one of the more variable parameters with respect to the field. Since the formation of the drift field is basically nothing more than a diffusion process, it is expected that the width and distribution of impurity atoms of the field itself are quite repeatable because of the careful control of diffusion time and temperature. Hence the configuration of the field itself should be fairly well consistent from cell to cell and would therefore not be expected to cause the variations in the observed radiation characteristics. The data seems to indicate that the inclusion of the drift field can have an adverse effect on the sensitivity of the cell open circuit voltage to bombardment by 1 MeV electrons, and further, that drift field cell configurations which provide low sensitivity of short circuit current to irradiation seem to give rise to cells which have a greater sensitivity of open circuit voltage to irradiation.

---

1) Wolf, M., "Drift Fields in Photovoltaic Solar Energy Converter Cells" Proc. IEEE, Vol. 51, No. 5, May 1963

VII. CONCLUSIONS AND RECOMMENDATIONS

Progress in the fabrication of drift field cells having the near optimum design has been steady and according to plan. The major difficulty encountered was precisely as predicted at the outset of the contract, namely the reduction of the final substrate thickness. In the early sample lots most of the cells were very small in area and inconsistencies occurred across the area of the cell. However, these difficulties were not noticeably detrimental to the cell performance and did not detract from the analytical value of studying drift field cell behavior in a radiation environment. As the technology of fabrication improved, larger area cells became more dominant and the last shipment of drift field cells was comprised of six 1x2 cm cells and two 1x1 cm cells. Thus any non-uniformity throughout this larger area would become more influential in the quality of the cell electrical characteristics.

At the present time the major cause of inconsistency is believed to be a bowing effect on the slices from which the cells are cut. During substrate removal, the bowing causes some areas of the cell to be lapped thinner than others and often times results in the slices being lapped or etched through to the epitaxial substrate, resulting in an unusable or very low efficiency cell. Careful control in the pre and post epitaxial heat treatment has helped to reduce the amount of slice bowing, but does not completely eliminate the problem. Alternate fabrication techniques such as utilization of smaller substrate blanks will be investigated in the next period to further minimize the effects of bowing.

It has been observed that the short circuit currents obtained from the drift field cells are quite close to what one would expect theoretically. The cell efficiencies for the most part, are slightly below that anticipated and it is expected that the average efficiency could be further increases through an increase in open circuit voltage.

It is possible that some process limitations exist with respect to the cell design being studied. There is some loss of efficiency in the drift field cells due to the rather high shunt currents, which seem at this time to exist in the body of the cell rather than at the edges as in normal field free cells. These body shunt paths may be a result of crystalline imperfections which propagate due to the strains originating at the substrate-epitaxi interface. The density of such defects, especially as a function of the distance normal to the plane of the interface, is probably dependent on the treatment of the slice subsiquent to the epitaxial deposition. Such things as lapping and heat trating will tend to increase propagation of defects. Controlled experiments could be done to obtain a measure of the effects of such treatment on the cell parameters. A preliminary experiment performed during the course of this contract to determine the effect of substrate thickness variation on the cell electrical parameters, showed that, in general, considerably better short circuit current, open circuit voltage and cell efficiency was obtained with thicker substrates. Theoretically one expects an increase in short circuit current with the thicker base region, but the observed increase in the voltage parameter is greater than theoretically expected and is hence indicative that there are additional factors present due to processing. Since the experiment was of a preliminary nature, further investigation along these lines are clearly indicated. Once the problem areas have been more precisely defined, methods can be found to circumvent, minimize, or eliminate them. It is quite likely that the utilization of a polish-etched surface in conjunction with an evaporated-sintered contacting technique will yield higher open circuit voltages as indicated by a preliminary experiment which compared the electrical characteristics of the cell type to those of lapped-surface, plated-contact cells.

Radiation experiments performed on drift field cells have yielded encouraging results. It has been shown that drift field cells can be designed so that they have higher efficiencies than high efficiency state-of-the-art field free cells after fluxes of 1 MeV electrons of the order of 10^{16} electrons per square centimeter. Also an interesting voltage effect has been observed which may lead to a more thorough understanding of the ramifications of the base region drift field on the cell operating efficiency, especially after irradiation by 1 MeV electrons.